

# Elucidation of Aqueous Solvent-Mediated Hydrogen-Transfer Reactions by ab Initio Molecular Dynamics and Nudged Elastic-Band Studies of NaBH<sub>4</sub> Hydrolysis

Ping Li,<sup>†</sup> Graeme Henkelman,<sup>‡</sup> John A. Keith,<sup>†</sup> and J. Karl Johnson\*,<sup>†,§</sup>

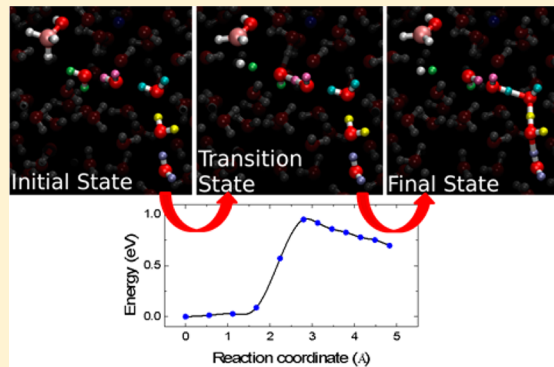
<sup>†</sup>Department of Chemical and Petroleum Engineering, University of Pittsburgh, Pittsburgh, Pennsylvania 15261, United States

<sup>‡</sup>Department of Chemistry, University of Texas at Austin, Austin, Texas 78712-0165, United States

<sup>§</sup>National Energy Technology Laboratory, 626 Cochran's Mill Road, Pittsburgh, Pennsylvania 15236, United States

## Supporting Information

**ABSTRACT:** The rational development of aqueous-phase catalysts is limited by a lack of fundamental understanding of the precise role of solvent molecules in the reactions. For deeper insight into these general processes, we carried out a detailed theoretical study of NaBH<sub>4</sub> hydrolysis to unravel a plethora of complex reaction pathways. Our study involves no *a priori* assumptions about individual reactant or product states, which are identified through a combination of ab initio molecular dynamics and nudged elastic-band methods. Snapshots of our computational modeling identify canonical reaction mechanisms whereby the aqueous environment facilitates proton and hydride transfers as well as solvent rearrangements extending across multiple layers of solvation. In addition to providing the most comprehensive computational study of NaBH<sub>4</sub> hydrolysis to date, the mechanisms presented herein are relevant for characterizing other reaction processes involving coupled proton-hydride reactions influenced by subtle changes in reaction environments (e.g., those that would be encountered in hydrogen evolution, water oxidation, and CO<sub>2</sub> conversion processes). This novel and unbiased quantum chemistry modeling approach shows great promise for computational elucidation of homogeneous phase chemistry.



## INTRODUCTION

Recent focus on renewable energy catalysis has reemphasized the need for improved fundamental understanding of proton, hydrogen, and hydride transfers in solution.<sup>1–7</sup> These reactions are often the critical steps in various biochemical processes,<sup>8</sup> hydrogen storage in chemical<sup>9</sup> and metal hydrides,<sup>10</sup> hydrogen evolution,<sup>11–14</sup> water oxidation,<sup>15–18</sup> and CO<sub>2</sub> reduction.<sup>11,19–23</sup> While first-principles quantum chemistry modeling can provide important insight into these processes, predictions from some of these approaches can be limited due to *a priori* assumptions about the role of solvent molecules and the precise reaction steps. For example, modeling a solution-phase reaction with only a few explicit water molecules may not correctly model the true role of the solvent. Furthermore, there is no guarantee that a user-defined reaction coordinate represents the actual reaction pathway. Robust and unbiased computational modeling approaches would elucidate complicated reaction mechanisms for the development of improved, economical, and versatile catalysts.

Such modeling can be employed to better understand sodium borohydride, which has a remarkably broad spectrum of uses.<sup>24–35</sup> NaBH<sub>4</sub> is safe to store and handle, and it is one of the least expensive metal hydrides commercially available (on a hydride equivalent basis). Chemists use it ubiquitously in

laboratories as a reducing agent for converting aldehydes and ketones into alcohols, and it has been widely studied for hydrogen storage since it was first synthesized by Schlesinger et al. in the early 1950s.<sup>36</sup> Many chemical processes use NaBH<sub>4</sub>, but atomic-scale aspects of its solution phase chemistry have remained poorly understood.<sup>37</sup> While hydrolysis reactions are often regarded as simple to carry out in a laboratory, atomic-scale NaBH<sub>4</sub> hydrolysis mechanisms have been controversial for more than a half century. The aforementioned versatility of NaBH<sub>4</sub> suggests that it may have even more undiscovered uses, but the rational development of new technologies that exploit subtle aqueous-phase phenomena necessitates new tools for deeper understanding.

Overall, one single chemical equation can compactly express NaBH<sub>4</sub> hydrolysis:



where  $x$  represents excess (undesirable) water, which decreases hydrogen storage density in a reaction system. Equation 1 reveals neither the subtlety of the fundamental molecular

Received: August 4, 2014

Revised: August 25, 2014

Published: September 9, 2014



mechanisms nor the practical difficulties of carrying out this reaction. This process only involves relatively small molecules, but as alluded to above, experimental hydrolysis mechanistic studies have neither been conclusive nor consistent with one another.<sup>37</sup> Moreover, many of the hypothesized reaction steps in NaBH<sub>4</sub> hydrolysis involve reactions between hydridic and protonic hydrogens, whose natures are certainly influenced by complex aqueous environments.<sup>38</sup>

These points make NaBH<sub>4</sub> an ideal system to study using state-of-the-art unbiased computational modeling. Although the detailed mechanisms in this study are directly relevant to hydrogen storage, one finds that the elementary reaction mechanisms that comprise eq 1 should also be applicable to other classes of chemical reactions involving proton and/or hydride transfers such as those mentioned above. In fact, when scrutinized with snapshots of the reaction mechanism from theory, we find that several elementary steps follow conventional (i.e., textbook) reaction mechanisms such as reductive eliminations and S<sub>N</sub>2 reactions. Not only that, but chemistry of boron atoms with an empty *p* orbital resembles that of conventional transition metal chemistry.

Our study differentiates and then categorizes the elementary reaction pathways encompassed in eq 1 to provide fundamental insight for better control over individual proton and hydride transfers in solution. To do this, we begin by briefly summarizing multiple experimental observations to highlight what is known and not known about NaBH<sub>4</sub> hydrolysis to show how this kind of theoretical modeling can predict and clarify unknown reaction mechanisms.

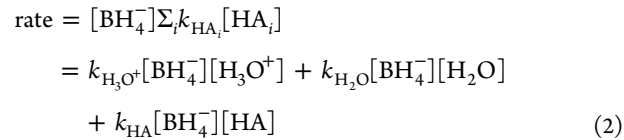
## PRIOR EXPERIMENTAL STUDIES ON NABH<sub>4</sub> HYDROLYSIS

NaBH<sub>4</sub> hydrolysis proceeds slowly without catalysis at ambient conditions. Previous work has often focused on improved kinetics and yields using metal catalysts<sup>39–51</sup> or steam hydrolysis.<sup>52–54</sup> The apparent activation energy for the uncatalyzed NaBH<sub>4</sub> hydrolysis reaction was reported to be  $1.02 \pm 0.10$  eV.<sup>55</sup> Activation energies with various heterogeneous catalysts range from about 0.3 to 0.8 eV.<sup>47–51</sup> The reaction rate, reaction mechanism and the hydrolysis end products are all dependent on the pH of the solution.<sup>24,37</sup> Acids have long been known to accelerate NaBH<sub>4</sub> hydrolysis, but there is still no complete description of the reaction mechanism, and some details of the initial steps remain inconclusive.<sup>24,37</sup>

Most experimental efforts aiming to identify BH<sub>4</sub><sup>-</sup> hydrolysis mechanisms were carried out more than 60 years ago.<sup>36,56–78</sup> Recent work has instead focused on engineering optimal reaction conditions and catalysts.<sup>39–41,43–54,79–85</sup> Experimental studies generally concluded that the rate-limiting step of the first H<sub>2</sub> generation step involves BH<sub>4</sub><sup>-</sup> protonation,<sup>59,67,69–71,73,77</sup> but there is disagreement over what is the product of the first elementary reaction step. On the basis of isotope kinetics studies, Davis et al. concluded the first product would be BH<sub>3</sub>,<sup>67,70</sup> while Mesmer and Jolly proposed it would be BH<sub>5</sub>.<sup>71</sup> Proton magnetic resonance studies have not been able to identify other intermediates, thereby suggesting that all subsequent reaction steps are very rapid.<sup>71</sup> Other products in BH<sub>4</sub><sup>-</sup> hydrolysis have been proposed including BH<sub>3</sub>OH<sup>-</sup>, BH<sub>2</sub>(OH)<sub>2</sub><sup>-</sup>, and BH(OH)<sub>3</sub><sup>-</sup>.<sup>57,58,61,65,68,73–76</sup> Gardiner and Collat characterized BH<sub>3</sub>OH<sup>-</sup> on the basis of <sup>11</sup>B NMR spectra and polarographic data.<sup>73,74</sup> Goubeau and Kalfass also reported BH<sub>3</sub>OH<sup>-</sup> formation observed by infrared spectra.<sup>65</sup> At the time

they claimed that the first hydrogen atom would leave BH<sub>4</sub><sup>-</sup> more rapidly than the other three hydrogen atoms, though later consensus formed that BH<sub>5</sub> formation is actually rate limiting. Mochalov et al. proposed that NaBH<sub>4</sub> hydrolysis in buffered solutions consisted of stepwise substitutions of B–H bonds in BH<sub>4</sub><sup>-</sup> with B–OH bonds.<sup>68,75,76</sup> Recent reviews summarize these earlier experiments in greater detail.<sup>24,37</sup>

The first step of BH<sub>4</sub><sup>-</sup> hydrolysis under acidic conditions was proposed to be first-order in the reactant according to



where HA<sub>i</sub> is a general acid.<sup>59,67,69,70,73,77</sup> The rate constant  $k_{\text{H}_3\text{O}^+}$  was reported to be  $(1.00 \pm 0.04) \times 10^6 \text{ M}^{-1} \text{ s}^{-1}$  by Davis et al. via iodate analysis,<sup>70</sup>  $2.5 \times 10^5 \text{ M}^{-1} \text{ s}^{-1}$  by Pecsok based on polarographic techniques,<sup>59</sup> and  $(9.9 \pm 0.03) \times 10^6 \text{ M}^{-1} \text{ s}^{-1}$  by Kreevoy and Hutchins from manometrical measurements.<sup>77</sup> Activation energies for the term have been reported by Pecsok,<sup>59</sup> Freund,<sup>64</sup> Stockmayer et al.,<sup>69</sup> and Gardiner et al.<sup>73</sup> to be 0.39, 0.31, 0.39  $\pm$  0.04, and 0.48  $\pm$  0.04 eV, respectively.

In summary, despite the copious experimental work on borohydride hydrolysis, there is a noticeable lack of understanding of the individual reaction steps and the role of aqueous environment in the reaction mechanisms. We will now demonstrate that periodic Kohn–Sham density functional theory (DFT) can be used to identify all of the essential elementary reaction steps for uncatalyzed NaBH<sub>4</sub> hydrolysis through a combination of high-temperature molecular dynamics and state-of-the-art transition state finding algorithms. We use this formalism to show that eq 1 involves as many as 16 elementary reaction steps, and we quantify all with their accompanying barriers. Surprisingly, we found that many of these reactions involve extensive proton shuttling across water networks that extend beyond the first solvation shell of the reactants. Again, while this study provides comprehensive insight into the chemistry of uncatalyzed NaBH<sub>4</sub> hydrolysis, we also make note of the versatile binding motifs found at boron, making this study also relevant for representing quintessential proton and hydride transfers in aqueous solution that might be facilitated with proteins, organometallics complexes, and nanomaterials.

## COMPUTATIONAL METHODS

First-principles periodic plane-wave DFT<sup>86,87</sup> calculations were carried out using the Vienna *ab initio* simulation package (VASP).<sup>88–91</sup> The calculations utilized the PW91 exchange correlation functional within the generalized gradient approximation (GGA)<sup>92,93</sup> as well as projector augmented wave (PAW) pseudopotentials on all atoms.<sup>94,95</sup> Plane wave cutoff energies were set to 520 eV after finding this gave well-converged structures and total energies. It is well-known that DFT with standard GGA functionals may give incorrect results for some systems, mainly because of delocalization and static correlation errors.<sup>96</sup> We note that while modeling liquid water with DFT is notoriously challenging,<sup>97–100</sup> the PW91 exchange-correlation functional gives reasonable structural, energetic, and transport properties for bulk liquid water in agreement with experiments.<sup>101</sup> Moreover, Leung et al. demonstrated that PW91 models of the water/formate ion system gave results in qualitative agreement with experimental

structural data.<sup>102</sup> Thus, this approach should provide predictive insights into the aqueous NaBH<sub>4</sub> system.

We tested the accuracy of the PW91 functional by comparing results with those from high-level *ab initio* calculations for two gas phase reactions that mimic elementary reaction steps found in our condensed phase calculations. We used second-order Møller–Plesset perturbation theory and coupled cluster CCSD(T)-F12b<sup>103</sup> because these methods are free from the delocalization and static correlation errors that plague DFT. We found that barrier heights from PW91 are within 0.2 eV of the CCSD(T)-F12b results, which is reasonable accuracy for a pure GGA approach. We expect that the mechanisms identified here will be accurate, although the barriers estimated from our PW91 calculations are not within chemical accuracy. Details of the calculations are given in the Supporting Information.

Born–Oppenheimer *ab initio* molecular dynamics (AIMD) calculations were carried out using VASP to identify candidate reaction mechanisms and reaction intermediates (see Supporting Information for details). We stress that unlike other first-principles quantum chemistry mechanistic studies<sup>104,105</sup> that have treated solvation with implicit continuum models<sup>106–108</sup> or mixed explicit/continuum models,<sup>109–113</sup> this approach allowed us to make no *a priori* assumptions about the number and types of intermediates or products. All reaction intermediates were observed naturally during the course of the AIMD simulations. Nudged elastic band (NEB) methods were then used to link these intermediates via reaction pathways determined by the computational algorithm, enabling us to see how and how many explicit water molecules participate in these aqueous-phase reactions. We note that Mattioli et al. recently used a combination of AIMD and NEB methods in a study to identify reaction pathways for oxygen evolution occurring on Co catalyst nanoparticles.<sup>114</sup>

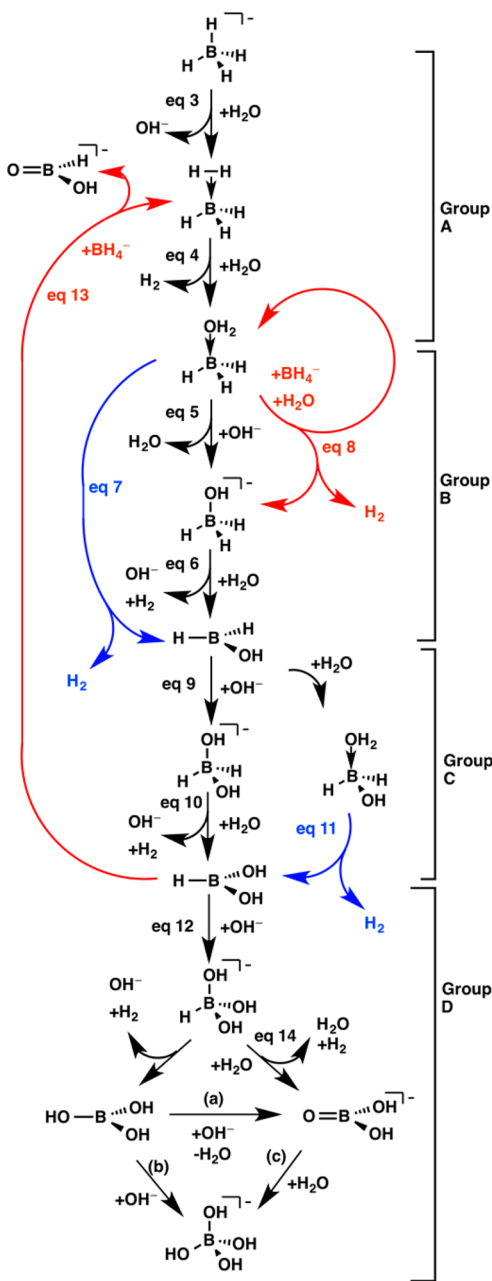
The size of our cubic AIMD simulation cell was 10 Å on each side. Three different compositions were modeled to account for concentration effects. Systems were constructed with one, two, or three NaBH<sub>4</sub> groups and 33, 31, or 29 H<sub>2</sub>O molecules, respectively, to give densities consistent with liquid-phase solutions. Multiple AIMD simulations were performed for 10 ps or more at a very high temperature (2000 K) to accelerate kinetics to generate a family of candidate reaction pathways. The temperature acceleration allowed more efficient exploration of reaction pathways and reduced the time trapped in local minima and therefore facilitated the identification of a larger number of reaction mechanisms than simulations at lower temperature for a given time interval. The reaction events observed in AIMD simulations were used to generate initial guesses for reactant and product states for NEB transition state calculations. We performed geometry optimizations at 0 K starting from structures obtained from AIMD simulations. Note that we are not identifying reaction rates through high-temperature AIMD because rates and the relative importance of competing pathways depend exponentially on temperature. Reaction pathways, which are independent of temperature, were then obtained using NEB methods at 0 K. Therefore, these data are not to free energies. The NEB calculations often yielded intermediate minima and these were often used as starting (or ending) points for refining the reaction pathways. Note that this approach is different from AIMD metadynamics procedures,<sup>115</sup> which also investigate chemical kinetics under the influence of solvation effects and provide estimates of the free energies of reaction,<sup>116–120</sup> but which require specification of constraints or collective variables that influence the selection

of the reaction pathway. We identified minimum-energy pathways involving both atomic and unit-cell degrees of freedom using the generalized solid-state nudged elastic band (G-SSNEB) method.<sup>121</sup> The G-SSNEB method was employed because the constant volume NEB (CVNEB) method typically failed to converge when using the local minima obtained from relaxation of the AIMD snapshots as the reaction pathway end points. We found that the relaxation of the volumes in the G-SSNEB facilitated convergence of the reaction pathways and we ascribe this to ensuring that the pressure within the liquid along the pathway is close to zero. To ensure G-SSNEB pathways were robust and realistic, we constructed CVNEB pathways based on the initial and final state geometries obtained from G-SSNEB calculations but requiring the cells to have cubic symmetry and to have the minimum volume encountered in the G-SSNEB pathway. The atom positions for the initial and final states in these CVNEB calculations were relaxed at the new cell volumes. This means that the G-SSNEB and CVNEB calculations did not have the same end points and hence were somewhat independent. The simulation cell lengths ranged from about 9.5 to 10.5 Å on each side in the CVNEB calculations. These values corresponded to the minimum volumes of the noncubic cells encountered in the G-SSNEB calculations. We used the climbing image NEB approach<sup>122,123</sup> with both G-SSNEB and CVNEB calculations. G-SSNEB has been successfully used for determining reaction pathways for solid–solid transitions.<sup>121</sup> This study is the first to show that it can also be used to study aqueous-phase reactions. We used the Quick-Min optimizer<sup>124</sup> for the NEB calculations, converging the reaction path until forces on all atoms were less than 0.03 eV/Å. We tested this convergence criterion by comparing the energies and geometries computed with a convergence criterion of 0.01 eV/Å for a representative pathway and found only a 0.02 eV decrease in the barrier height for the tighter convergence. Note that we do not apply zero-point energy corrections or account for nuclear quantum effects in any way. These corrections would decrease the barriers but are not likely to change the pathways significantly. It is not the goal of this work to report highly accurate values for the reaction barriers (indeed, standard GGA DFT is not the appropriate tool for such a goal). Our results give mechanistic insight into the complex liquid-phase reactions that have not been identified previously. In principle, our results could be used to construct collective variables for metadynamics simulations that could include entropy and nuclear quantum effects (e.g., through the path integral formalism).

## RESULTS AND DISCUSSION

Scheme 1 summarizes elementary reaction steps identified for NaBH<sub>4</sub> hydrolysis. As noted above, we computed pathways using both G-SSNEB and CVNEB methods. Both found essentially identical sets of reaction pathways in terms of the apparent intermediate images, which indicates that the pathways identified are realistic and robust. The barrier heights computed from the two methods are always in qualitative agreement, but they quantitatively differed from each other by as much as 0.28 eV and an average absolute difference of 0.17 eV. The reaction energies are in worse agreement, differing by as much as 0.52 eV, average absolute difference of 0.23 eV (see Supporting Information Table S1). These differences in energies appear mainly to be due to solvent rearrangements. From this we infer that one should not think about a single reaction barrier, but rather consider an ensemble of barriers

**Scheme 1. Reaction Steps for the Uncatalyzed Hydrolysis of  $\text{NaBH}_4$  Studied in This Work<sup>a</sup>**



<sup>a</sup>Discussions of reactions are organized into groups A–D in the main text. Black lines show reactions between hydroxyborates and  $\text{H}_2\text{O}$ , blue lines show intramolecular reactions, and red lines indicate reactions between two borate species. Donor–acceptor bonds to the boron are denoted with an arrow.

depending on the specific configuration of the solvent. However, the basic features of the mechanisms appear to be robust, so that the pathways may be taken to be representative of what is actually occurring in the solution. We note that the uncertainty in these barriers is on par with the accuracies of computed barrier heights from DFT (of 0.2–0.3 eV). For brevity, we report CVNEB data for the remainder of this paper, while the Supporting Information contains comparisons between G-SSNEB and CVNEB reaction energy profiles (Supporting Information, Figures S2–S4) and a tabulation of

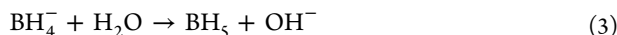
all calculated barrier heights and reaction energies (Supporting Information, Table S1).

Over the course of this study, we found that elementary hydrolysis steps involved complex solvent rearrangements at each step of the reaction, particularly around  $\text{OH}^-$  groups. AIMD simulations captured relatively long-range proton shuttling (of more than 8 Å), in agreement with expectations from experimentally observed structure of protons in aqueous solution.<sup>125</sup> Previous simulations have modeled proton relays in chemical reactions using relatively small numbers of explicit water molecules,<sup>112,113</sup> but in our case the long relays we have observed could not have been modeled this way without *a priori* knowledge of the pathway or the number of water molecules involved in the process. Although our approach does not calculate free energy barriers and therefore is not directly comparable to experimental observation, the sequentially linked images within the NEB calculations provide a descriptive illustration of each reaction pathway from start to finish. Furthermore, as with any process involving complex solvent rearrangements, ensembles of pathways should also be assumed to be in play. These ensembles may be more readily classified and characterized based on the pathways presented in this study.

For method validation, we first determined the energy barrier for the first step of the  $\text{NaBH}_4$  hydrolysis reaction under acidic conditions and then compared that result with experimentally known activation energies. Again, the experimentally observed enthalpy or free energy activation energies will not be exactly the same as energy barrier at zero kelvin that we calculate. Nevertheless, the reaction barrier calculated from our CVNEB calculations (see Figure S5 in the Supporting Information) is 0.50 eV, a value in good agreement with the high end of experimentally observed activation energies ranging from 0.31 to 0.48 eV.<sup>59,64,69,73</sup> Interestingly, the initial state for the reaction has  $\text{H}_3\text{O}^+$  and  $\text{BH}_4^-$  not being nearest neighbors but *next*-nearest neighbors. Repeated attempts to relax  $\text{H}_3\text{O}^+$  to a position immediately besides  $\text{BH}_4^-$  always resulted in proton shuttling off the hydronium onto an  $\text{H}_2\text{O}$  molecule in the second solvation shell of the  $\text{BH}_4^-$  anion. Proton hopping is a recurring theme in most of these reaction pathways. Additionally, the Na cation was found to be only an observer in all reaction processes.

As a second validation test, we estimated the overall reaction enthalpy for the  $\text{NaBH}_4$  hydrolysis at room temperature using our DFT approach and compared these results with experimental data. Recent experimental values for  $\text{NaBH}_4$  reacting to form  $\text{NaB}(\text{OH})_4$  are  $-2.18 \pm 0.11$  eV from Zhang et al.<sup>126</sup> and  $-2.45$  eV from Damjanović et al.<sup>127</sup> The reaction enthalpy was estimated by performing AIMD simulations of the reactant ( $\text{NaBH}_4 + 33\text{H}_2\text{O}$ ) and the product ( $\text{NaB}(\text{OH})_4 + 29\text{H}_2\text{O}$ , assuming ideal gas behavior for four  $\text{H}_2$  molecules) at 300 K. The two AIMD simulations for each case ran for about 40 ps, with the first 5 ps used for equilibration. The average energies for each system were estimated by averaging the energies of 40 snapshots for both the reactant and product simulations. This resulted in an estimated enthalpy change for  $\text{NaBH}_4$  hydrolysis of  $-1.80 \pm 0.34$  eV  $\text{NaBH}_4$ , in reasonable agreement with experimental values.

**Reactions Between Hydroxyborates  $\text{BH}_{4-x}(\text{OH})_x$  ( $x = 0, 1, 2, 3$ ) and  $\text{H}_2\text{O}$ . Reaction Group A.** The first step in the uncatalyzed hydrolysis of  $\text{NaBH}_4$  is proton donation from water to the  $\text{BH}_4^-$  group (eq 3). The result of this shuttling proton transfer is an  $\text{H}_2$  molecule bound to the B atom.



Note that this is fundamentally a protonation that converts a covalent bond into a donor–acceptor bond. Figure S6 of the Supporting Information shows the CVNEB minimum-energy reaction pathway for this process. While this elementary step has been identified experimentally,<sup>71,77</sup> the energy barrier for this process until now has been unknown. We calculate this energy barrier to be 1.03 eV, which is consistent with the experimental observation that NaBH<sub>4</sub> hydrolysis in solution is very slow in the absence of protons in solution at room temperature.<sup>52</sup> Figure 1 illustrates the structures of the initial, transition, and final states (see the corresponding movie in the Supporting Information).

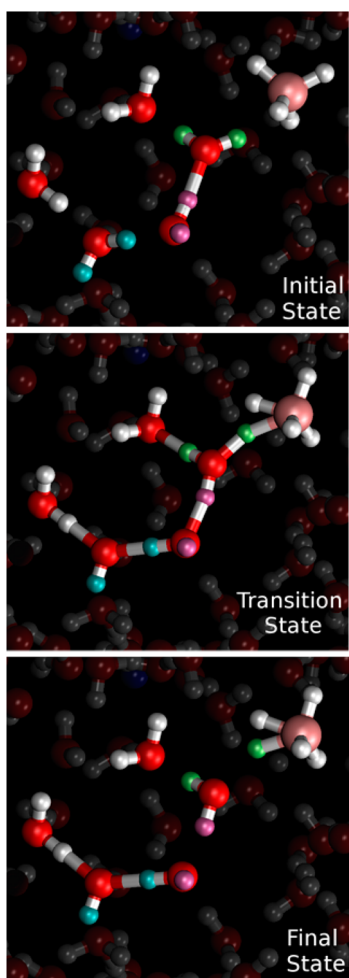


**Figure 1.** Structures of the initial, transition, and final states for H<sub>2</sub> formation at a donor–acceptor bonding site (eq 3). Molecules participating in the chemical reaction are highlighted, while molecules not participating in chemical reactions are semitransparent (this convention is also used in other figures). H atoms participating in proton transfers are colored to highlight the overall proton-transfer process. Red atoms are oxygen, the pink atom is boron, and hydrogens not participating in the reaction are white.

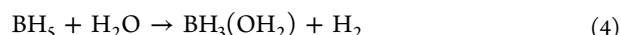
The reactant state for this process has a tetrahedral BH<sub>4</sub><sup>-</sup> ion retaining its four-coordinate structure with the formed H<sub>2</sub> bound via a three-center two-electron (3c-2e) bond, a bonding motif commonly found in organometallic complexes. Five H<sub>2</sub>O molecules form a chain to facilitate the overall proton transfer. The H<sub>2</sub>O closest to BH<sub>4</sub><sup>-</sup> in the initial state has an O–H bond

pointing to BH<sub>4</sub><sup>-</sup> that increased from ~1.0 Å to 1.4 Å at the transition state. From the transition state to the final state, one sees proton shuttling across the five water molecules resulting in the OH<sup>-</sup> ion being coordinated by hydrogen bonds with surrounding water molecules. The OH<sup>-</sup> is separated from the BH<sub>5</sub> group by about two H<sub>2</sub>O solvation layers (with a O–B distance of 7.4 Å, see Supporting Information). Long-distance proton shuttling was also observed in AIMD simulations for this reaction. A movie showing the reaction involving proton hopping among six different water molecules is provided in the Supporting Information. We sometimes observed the recombination of the BH<sub>5</sub> + OH<sup>-</sup> product state to the BH<sub>4</sub><sup>-</sup> + H<sub>2</sub>O initial state in our AIMD simulations when BH<sub>5</sub> and OH<sup>-</sup> were close proximity, that is, if proton shuttling did not result in the OH<sup>-</sup> group being effectively moved away from BH<sub>5</sub>.

We note in passing that the pH changes in our simulations as the reaction proceeds, for example, through the generation of an OH<sup>-</sup> group through eq 3, which is not the case for experiments in buffered solutions.

Our calculations show that BH<sub>5</sub> is a metastable state with C<sub>s</sub> symmetry (analogous to CH<sub>5</sub><sup>+</sup>), agreeing with previous studies.<sup>77,128,129</sup> This species was aptly identified as H<sub>2</sub>BH<sub>3</sub> by Kreevoy et al.,<sup>77</sup> because it has two relatively long and three normal B–H bond lengths, which distinguish the donor–acceptor complex involving BH<sub>3</sub> and H<sub>2</sub>. This moiety evolves molecular hydrogen in the subsequent reaction. Notably, the OH<sup>-</sup> byproduct from eq 3 is hydrated by four H<sub>2</sub>O molecules in the final state, as shown in Figure S7 in the Supporting Information (only two solvent H<sub>2</sub>O molecules are shown in the bottom panel of Figure 1 for clarity). This agrees with reports that OH(H<sub>2</sub>O)<sub>4</sub><sup>-</sup> is the most stable structure of OH<sup>-</sup> in aqueous solution.<sup>130,131</sup>

The next reaction step had BH<sub>5</sub> effectively undergoing an S<sub>N</sub>2 reaction to release H<sub>2</sub> and form a BH<sub>3</sub>(OH<sub>2</sub>) complex.



BH<sub>5</sub> dissociation has been studied previously.<sup>77,128,129,132,133</sup> Kreevoy and Hutchins proposed H<sub>2</sub>BH<sub>3</sub> → H<sub>2</sub> + BH<sub>3</sub> as the pathway based on kinetic data for acidic aqueous BH<sub>4</sub><sup>-</sup> hydrolysis.<sup>77</sup> Willem investigated the two-step process BH<sub>4</sub><sup>-</sup> + H<sup>+</sup> → BH<sub>5</sub> → BH<sub>3</sub> + H<sub>2</sub> via permutational analysis of experimental data.<sup>129</sup> Theoretical studies by Hoheisel and Kutzelnigg<sup>132</sup> and Stanton et al.<sup>133</sup> considered dissociation of gas-phase BH<sub>5</sub> to BH<sub>3</sub> and H<sub>2</sub>, but solvation effects were not considered. Pepperberg et al. also modeled BH<sub>3</sub>(OH<sub>2</sub>) as a product of BH<sub>5</sub> dissociation in a gas-phase molecular orbital study.<sup>128</sup> Because of the relatively limited computational resources available at the time, these early theoretical studies had to use very small basis sets known to provide unreliable energetics. Our AIMD calculations at 300 K indicate that BH<sub>3</sub> is highly reactive in aqueous solution and rapidly binds with H<sub>2</sub>O to generate BH<sub>3</sub>(OH<sub>2</sub>) within 1 ps. The minimum-energy pathway for eq 4 is shown in Figure S8 of the Supporting Information; the energy barrier is 0.42 eV, while the overall reaction is exothermic by 0.56 eV. The structures of initial, transition, and final states are shown in Figure 2. At the transition state, BH<sub>5</sub> dissociates into H<sub>2</sub> and planar BH<sub>3</sub>, which is known to exist in the gaseous state.<sup>60</sup> BH<sub>3</sub> then rapidly combines with a H<sub>2</sub>O molecule to form BH<sub>3</sub>(OH<sub>2</sub>).

**Reaction Group B.** BH<sub>3</sub>(OH<sub>2</sub>) can subsequently react via at least three different routes (Scheme 1). Previous studies on acidic NaBH<sub>4</sub> hydrolysis have simplified the reaction to BH<sub>3</sub> + 3H<sub>2</sub>O → 3H<sub>2</sub> + B(OH)<sub>3</sub> by assuming intermediate steps were

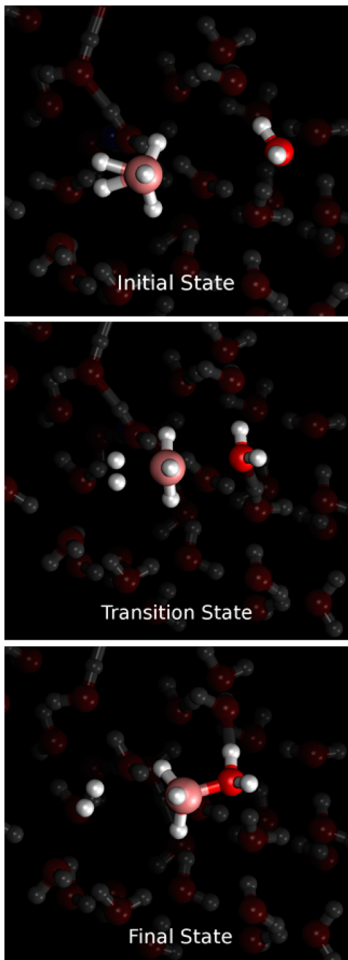
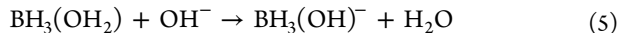


**Figure 2.** Structures of the initial, transition, and final states for the  $S_N2$  reaction releasing  $H_2$  from  $BH_5$  (eq 4, see Supporting Information, Figure S8 for the CVNEB profile).

fast.<sup>134</sup> This has been considered a reasonable approximation since no intermediates were readily observed.<sup>67,71,77</sup> However, other studies described the reaction as occurring in a stepwise fashion, depending on the pH of solution.<sup>73,74,78</sup> To clarify which pathways are more relevant, we first consider the pathway involving proton abstraction by  $OH^-$ .



Note that the requisite  $OH^-$  anion was generated in the initial reaction step, eq 3, making this process self-propagating. Our CVNEB calculations indicate that the energy barrier for eq 5 is very small, 0.03 eV, showing that this reaction is very fast. This result can be interpreted to explain why  $BH_3(OH_2)$  in basic solutions has been very challenging to observe. Our results agree with the experimental work of Gardiner and Collat, who proposed that  $BH_3(OH)^-$  is energetically more stable than  $BH_3(OH_2)$  based on ionic strength effects on reaction rates.<sup>72,73</sup> On the other hand, the very small barrier found in our calculations refutes the recent proposal of Andrieux et al., that  $BH_3 + OH^- \rightarrow BH_3(OH)^-$  is one of two rate-determining steps for the acidic hydrolysis of  $NaBH_4$  (the other being the initial generation of  $H_2$  from  $BH_4^- + H_3O^+ \rightarrow BH_3 + H_2O + H_2$ ).<sup>55</sup>

After crossing an effectively insignificant barrier for deprotonation, the reaction is downhill by 0.57 eV (Supporting

Information, Figure S9). Proton donation from  $BH_3(OH_2)$  to  $OH^-$  may occur through proton shuttling involving a chain of water molecules in a Grotthuss-like mechanism<sup>135</sup> shown in Figure 3 (see also the movie in the Supporting Information).

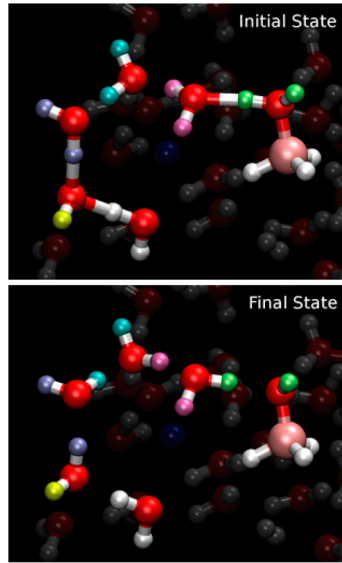
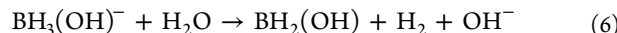


**Figure 3.** Structures of the initial and final states deprotonation of  $BH_3(OH_2)$  (eq 5, see Supporting Information, Figure S9 for CVNEB profile). Protons in  $H_2O$  molecules participating in the reaction are colored to highlight the proton-transfer process.

Owing to the low barrier, our NEB calculations found no discernible transition state for this process. The initial state identified from our calculations consisted of  $OH^-$  (identified by the yellow H atom in Figure 3) located about three nearest neighbors away from the  $BH_3(OH_2)$ . The  $H_2O$  moiety in  $BH_3(OH_2)$  (H atoms colored green) donates a proton into solution, leading to multiple proton transfers (purple, light blue, dark blue) to the  $OH^-$ . Overall, our modeling captures a total proton shuttling distance larger than 8 Å, adding each leg of the proton hop (i.e., not straight line beginning to ending positions).

Continuing on from  $BH_3OH^-$ , we found two possible pathways for producing  $H_2$  from  $BH_3(OH)^-$  and water through the reaction



The first mechanism, which we label as mechanism (i), involves a hydride on  $BH_3(OH)^-$  reacting directly with a proton on  $H_2O$  to form  $H_2$ , which is then released into solution. This  $H_2$  formation mechanism differs from that in eq 3, where the  $H_2$  here is released into solution rather than retained by the 3c-2e donor–acceptor bond in  $BH_5$ . The minimum-energy pathway and structures of the initial, transition, and final states are shown in Figure S10 (see the Supporting Information) and Figure 4, respectively. The barrier for this process is 0.95 eV from CVNEB calculations (Supporting Information, Figure S10). The distance between the hydride on  $BH_3OH^-$  and the proton on the neighboring  $H_2O$  begins at 1.71 Å in the initial state, changes to 0.80 Å at the transition state, and then ends at 0.75 Å in the final state (matching the gas phase  $H_2$  bond length calculated from our DFT method). As seen previously, protons hop along a water chain as shown in Figure 4 (see also the movie in the Supporting Information), culminating in  $OH^-$

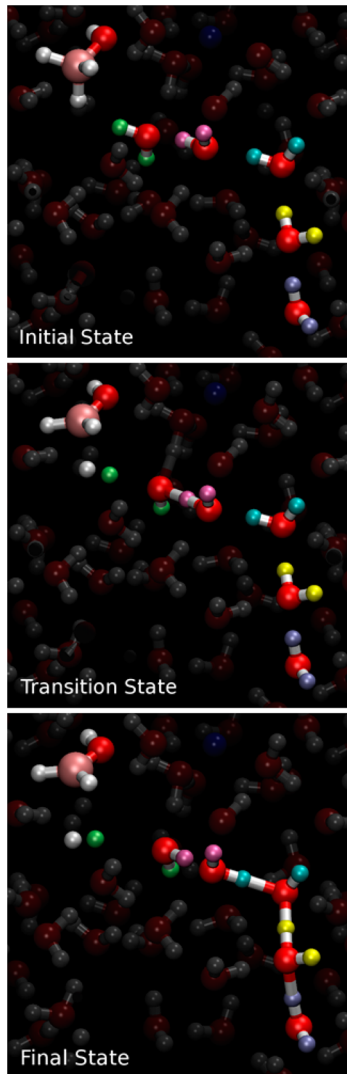


**Figure 4.** Structures of the initial, transition, and final states for hydrolysis of  $\text{BH}_3(\text{OH})^-$  by mechanism (i) (see eq 6, Supporting Information, Figure S10). Protons in  $\text{H}_2\text{O}$  molecules participating in the reaction are colored to highlight the proton-transfer process.

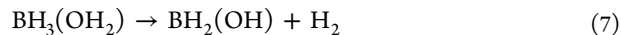
being produced about three nearest-neighbor water molecules away from the  $\text{BH}_2(\text{OH})$  product.

We also observed another pathway, mechanism (ii), whereby water autoionization first produces  $\text{H}_3\text{O}^+$ , which subsequently transfers a proton to  $\text{BH}_3(\text{OH})^-$  via proton shuttling, resulting in an overall coupled proton-hydride reaction similar to mechanism (i). The barrier for this process is higher (1.23 eV) than that for mechanism (i). The reaction barrier is shown in Figure S11 (see the Supporting Information) and the initial, transition, and final state configurations are shown in Figure S12 (see the Supporting Information). This process is effectively a collection of the water autoionization,<sup>136–139</sup> proton hopping, and  $\text{H}_2$  formation reaction steps. The reaction pathway involves the formation of a solvated Zundel cation ( $\text{H}_5\text{O}_2^+$ , Supporting Information, Figure S13), before the transition state (see the corresponding movie in the Supporting Information). More discussion is found in the Supporting Information.

Di Pietro et al.<sup>140</sup> previously studied hydrolysis of  $\text{BH}_4^-$  using AIMD in the Blue Moon ensemble<sup>141</sup> as part of their approach to investigating hydrolysis of diborane.<sup>140</sup> Such simulations

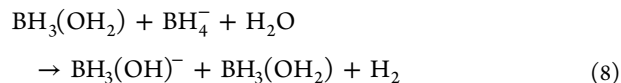
necessitate the specification of a reaction coordinate. In this case, they specified the B–O distance as the reaction coordinate and determined that  $\text{BH}_4^-$  hydrolysis proceeded without a significant barrier via a single reaction step:  $\text{BH}_4^- + 2\text{H}_2\text{O} \rightarrow \text{BH}_2(\text{OH}) + 2\text{H}_2 + \text{OH}^-$ . We note that this reaction is inconsistent with experimental findings<sup>55,71,77</sup> and was never observed in our unconstrained AIMD simulations. Our NEB calculations indicate that the above reaction is actually the sum of four elementary reaction steps given by eq 3 through 6. Therefore, it is highly unlikely to occur. The incorrect barrier observed by Di Pietro et al. is likely an artifact of using an incorrect reaction coordinate, similarly to what was observed by Mones and Csányi for a much simpler reaction.<sup>142</sup> This illustrates both the danger of using constrained AIMD or potential of mean force simulations without correct knowledge of the reaction pathway, as well as the robustness of our computational approach in eluding such problems.

We identified a pathway for production of  $\text{H}_2$  directly from  $\text{BH}_3(\text{OH}_2)$  through reductive elimination of  $\text{H}_2$  to produce  $\text{BH}_2(\text{OH})$ .



The transition state involves proton transfer from the  $-\text{OH}_2$  moiety to a hydride on the  $-\text{BH}_3$  moiety. Once  $\text{H}_2$  is formed, it spontaneously departs into solution. The  $\text{BH}_2(\text{OH})$  product shown in Figure 5 is the same three-coordinated planar structure as the products for the two mechanisms identified for eq 6. The barrier for this process is 1.44 eV (Supporting Information, Figure S14), and Figure 5 shows the initial, transition, and final states (see also the corresponding movie in the Supporting Information).

Another reaction mechanism involves hydrolysis of  $\text{BH}_3(\text{OH}_2)$  facilitated by a  $\text{BH}_4^-$  ion:



This reaction transforms  $\text{BH}_3(\text{OH}_2)$  to  $\text{BH}_3(\text{OH})^-$  and  $\text{BH}_4^-/\text{H}_2\text{O}$  to  $\text{BH}_3(\text{OH}_2)$  in a single complex pathway with an energy barrier of 1.31 eV (Supporting Information, Figure S15). This reaction involves proton transfer across five  $\text{H}_2\text{O}$  molecules, including the one in  $\text{BH}_3(\text{OH}_2)$ , as shown in Figure 6 (see also the corresponding movie in the Supporting Information). Interestingly, after the  $\text{BH}_3(\text{OH}_2)$  reactant species releases a proton to generate  $\text{H}_2$  on the other B atom, a water molecule simultaneously acts as a nucleophile in this process to allow  $\text{H}_2$  to be released via an  $\text{S}_{\text{N}}2$  reaction. The net reaction is the same as the sum of the three reactions given by eqs 3–5; the calculated barriers for these individual reactions are 1.03, 0.42, and 0.03 eV, respectively. However, the barrier for the concerted process shown in eq 8 is 1.31 eV, which is considerably higher than the highest barrier for any of the three steps. A detailed microkinetic modeling of these reactions would identify which pathway would be more favorable overall at what concentrations, but such a study is beyond the scope of this work.

We briefly summarize this collection of four mechanisms that generate  $\text{H}_2$  from  $\text{BH}_3(\text{OH}_2)$ . The first two involve  $\text{BH}_3(\text{OH}_2)$  undergoing a spontaneous deprotonation to form  $\text{BH}_3(\text{OH})^-$ . The key mechanisms are (1)  $\text{H}_2\text{O}$  reacts with  $\text{BH}_3(\text{OH})^-$  to form  $\text{H}_2$  (barrier = 0.95 eV); (2) autoionization of  $\text{H}_2\text{O}$  to form  $\text{H}_3\text{O}^+$  (and  $\text{OH}^-$ ), followed by proton transfer from  $\text{H}_3\text{O}^+$  to  $\text{BH}_3(\text{OH})^-$  to release  $\text{H}_2$  (barrier = 1.23 eV); (3) direct  $\text{H}_2$

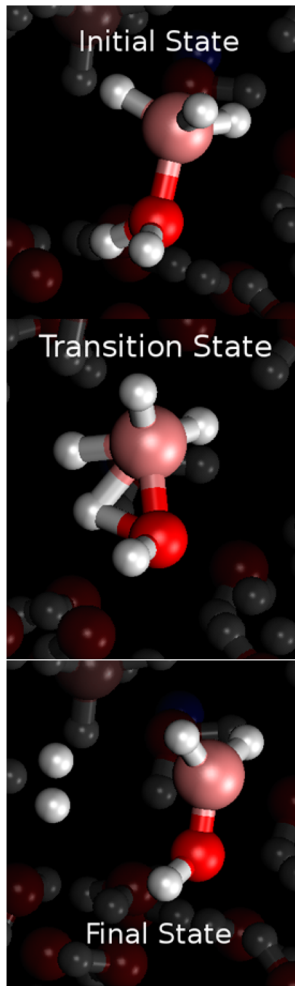
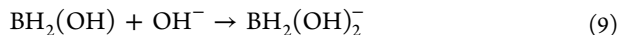


**Figure 5.** Structures of the initial, transition, and final states for the intramolecular reconstruction of  $\text{BH}_3(\text{OH}_2)$  to  $\text{BH}_2(\text{OH})$  (eq 7 and Supporting Information, Figure S14).

elimination from  $\text{BH}_3(\text{OH}_2)$  to form  $\text{BH}_2(\text{OH})$  (barrier = 1.44 eV); and (4) a concerted mechanism effectively carrying out eqs 4 and 5, but in the presence of another  $\text{BH}_4^-$  molecule (barrier = 1.31 eV). Notably, when  $\text{H}_2$  forms in the presence of an empty orbital on B,  $\text{H}_2$  can remain bound to B until it undergoes an  $\text{S}_{\text{N}}2$  reaction with  $\text{H}_2\text{O}$ . A similar design principle could be employed to facilitate other chemical reaction processes as well. Immediately after  $\text{H}_2$  elimination,  $\text{H}_2$  spontaneously is released into solution. Process (3) is much less energetically favorable than either solvent-assisted processes (1) and (2), however.

**Reaction Group C.** We found two pathways that can form  $\text{H}_2$  from the planar  $\text{BH}_2(\text{OH})$  intermediate product. The first pathway involves two reaction steps, and the first step involves  $\text{OH}^-$  addition to  $\text{BH}_2(\text{OH})$  to form a tetrahedral complex:



The energy barrier for this reaction (Supporting Information, Figure S16) is only 0.13 eV. When  $\text{BH}_2(\text{OH})$  is near a solvated  $\text{OH}^-$  approximately two nearest-neighbor water molecules away (local minimum, top panel in Figure 7), the  $\text{H}_2\text{O}$  adjacent to  $\text{BH}_2(\text{OH})$  can deprotonate, facilitating the net  $\text{OH}^-$  addition. This process involves the formation of a relatively strong B–O bond, making this a highly exothermic step that is energetically downhill by 0.74 eV (see the Supporting

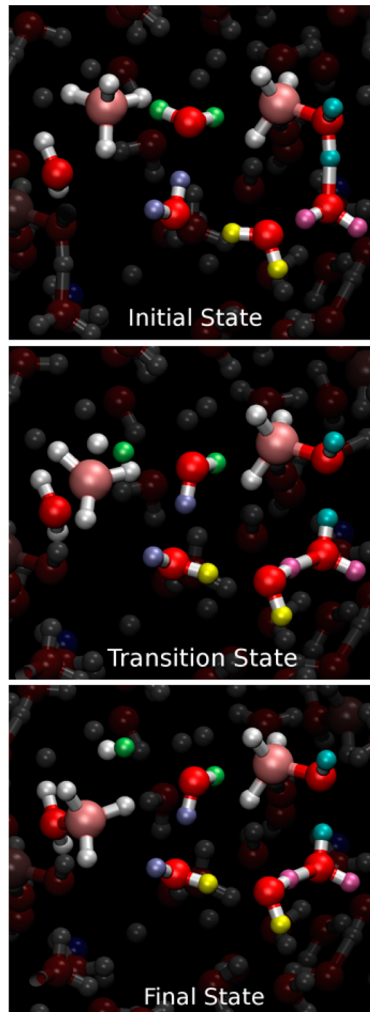


**Figure 6.** Structures of the initial, transition, and final states for reaction between  $\text{BH}_3(\text{OH}_2)$  and  $\text{BH}_4^-$  (eq 8 and the Supporting Information, Figure S15).

Information, Figure S16). Again, explicit solvation plays a critical step in catalyzing this reaction process.

$\text{BH}_2(\text{OH})_2^-$  from eq 9 in turn can react with  $\text{H}_2\text{O}$  to liberate  $\text{H}_2$  with a calculated barrier of 1.02 eV (Supporting Information, Figure S16) according to



This reaction is exothermic by 0.45 eV and proceeds via a proton plus hydride mechanism that directly releases  $\text{H}_2$  as was found for the process in eq 6. The hydroxyl ion product is effectively transported away from the reaction center via a Grotthuss-like mechanism shown in Figure 8. The similar mechanisms for eqs 6 and 10 suggest that hydroxyborates  $\text{BH}_{4-x}(\text{OH})_x^-$  ( $x = 1, 2$ ) can react with  $\text{H}_2\text{O}$  to produce  $\text{H}_2$  and three-coordinated planar  $\text{BH}_{3-y}(\text{OH})_y$  ( $y = 1, 2$ ) species. Furthermore, we find that both  $\text{BH}_2\text{OH}$  and  $\text{BH}(\text{OH})_2$  are transient species. In aqueous solvent, they would rapidly form  $\text{BH}_2\text{OH}-\text{OH}_2$  and  $\text{BH}(\text{OH})_2-\text{OH}_2$  complexes. In basic solutions they may instead combine with  $\text{OH}^-$  to form hydroxyborate anions.

The second  $\text{BH}_2(\text{OH})$  hydrolysis pathway that we identified begins with the (barrierless) formation of  $\text{BH}_2(\text{OH})(\text{OH}_2)$  from  $\text{BH}_2(\text{OH})$  and  $\text{H}_2\text{O}$ . This is energetically preferable to forming  $\text{BH}_2(\text{OH})_2^-$  from  $\text{BH}_2(\text{OH})$  and  $\text{OH}^-$ . The tetrahedral

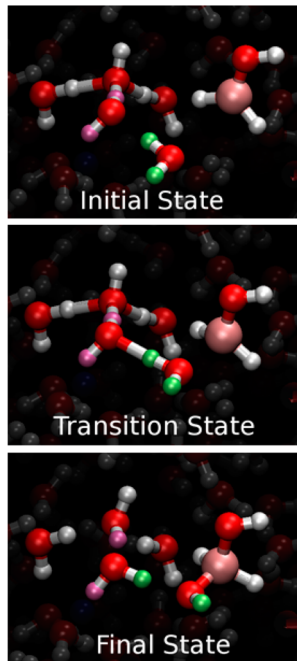


**Figure 7.** Structures of the initial, transition, and final states for  $\text{OH}^-$  addition to  $\text{BH}_2(\text{OH})$  to form  $\text{BH}_2(\text{OH})_2^-$  (eq 9 and Supporting Information, Figure S16).

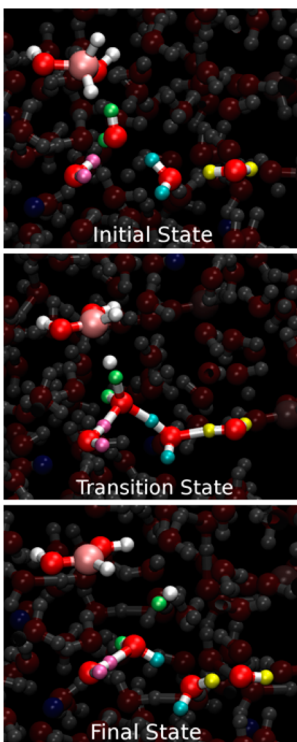
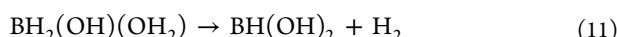


**Figure 8.** Structures of the initial, transition, and final states in hydrolysis of  $\text{BH}_2(\text{OH})_2^-$  to  $\text{BH}(\text{OH})_2$  (eq 10 and Supporting Information, Figure S16).

complex then undergoes a direct  $\text{H}_2$  elimination to produce  $\text{H}_2$  and three-coordinate  $\text{BH}(\text{OH})_2$  in a single step, rather than the stepwise process of eqs 9 and 10.



The energy barrier for this step is 1.43 eV (see the Supporting Information, Figure S18). Figure 9 illustrates the intramolecular

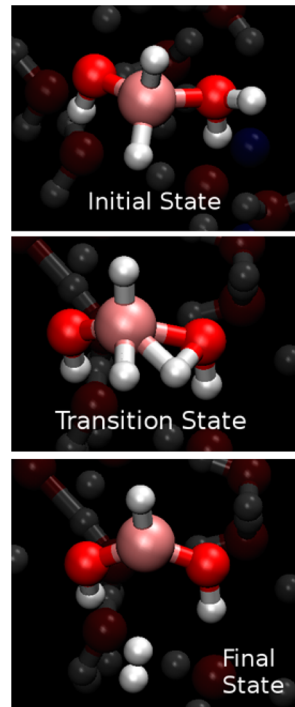


**Figure 9.** Structure of the initial, transition, and final states of  $\text{H}_2$  elimination from  $\text{BH}_2(\text{OH})(\text{OH}_2)$  (eq 11 and Supporting Information, Figure S17).

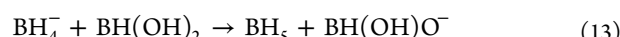
reconstruction process, where one  $\text{H}$  atom in the  $\text{H}_2\text{O}$  moiety is shared by both the  $\text{B}$  and  $\text{O}$  atoms at the transition state. This is similar to the pathway identified for eq 7, illustrated in Figure 5. Although this reaction is a single-step pathway, we believe that the two-step pathway given in eqs 9 and 10 would typically be preferred at moderate temperatures with sufficient concentrations of hydroxyl ions because the first step, eq 9, should be very rapid and essentially irreversible.

**Reaction Group D.** The uncharged  $\text{BH}(\text{OH})_2$  species may combine with  $\text{OH}^-$  to produce  $\text{BH}(\text{OH})_3^-$  as  $\text{OH}^-$  moves toward  $\text{BH}(\text{OH})_2$  through a proton-transfer mechanism similar to the hydroxyl addition to  $\text{BH}_2(\text{OH})$  of eq 9 (Figure 7).



The energy barrier of this step (0.45 eV, see the Supporting Information, Figure S19) is considerably larger than the barrier for eq 9 (0.13 eV). Likewise, adding the second hydroxyl group to the  $\text{B}$  atom (eq 9) is considerably more exothermic ( $-0.74$  eV) compared to adding a third hydroxyl group ( $-0.15$  eV). The structures of initial, transition and final states are shown in Figure 10. The hydroxyl group is separated by a solvation shell from the  $\text{BH}(\text{OH})_2$  molecule in the initial state (Figure 10).  $\text{OH}^-$  attachment takes place through proton transfer from the  $\text{H}_2\text{O}$  closest to  $\text{BH}(\text{OH})_2$ .

The uncharged  $\text{BH}(\text{OH})_2$  species may also react with  $\text{BH}_4^-$  to form  $\text{BH}_5^-$ :



This reaction's barrier is 0.91 eV (see the Supporting Information, Figure S20), which is lower than the barrier for the reaction between  $\text{H}_2\text{O}$  and  $\text{BH}_4^-$  shown earlier in eq 3 (1.03

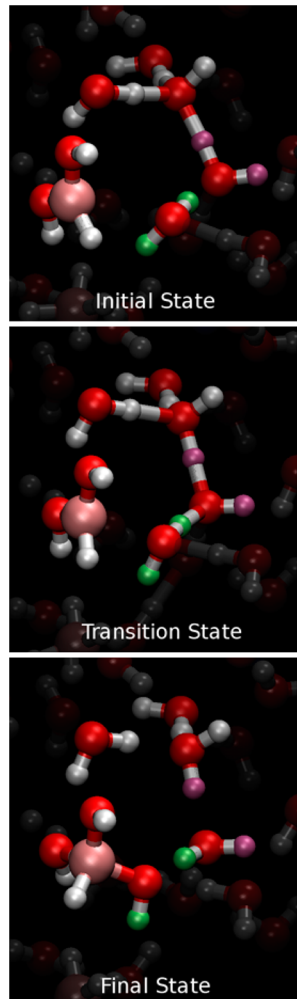
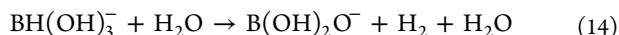


**Figure 10.** Structure of the initial, transition, and final states for  $\text{OH}^-$  addition to  $\text{BH}(\text{OH})_2$  to form  $\text{BH}(\text{OH})_3^-$  (eq 12 and Supporting Information, Figure S19).

eV, see the Supporting Information, Figure S6). Hence, eq 13 offers a competitive alternate pathway to eq 3. However, the concentration of  $\text{B}(\text{OH})_2$  is likely to be very low in solutions containing  $\text{OH}^-$ , since the reaction consuming  $\text{BH}(\text{OH})_2$  via eq 12 has a low energy barrier. Moreover, the concentration of the proton donor in eq 3,  $\text{H}_2\text{O}$ , will dwarf the concentration of the proton donor in eq 13,  $\text{BH}(\text{OH})_2$ , so that we expect eq 3 to normally be in play in aqueous solutions. The reaction pathway for eq 13 is relatively simple and does not involve solvent molecules participating in the reaction (see Figure 11 and the corresponding movie in the Supporting Information).

The reaction mechanism between  $\text{BH}(\text{OH})_3^-$  and  $\text{H}_2\text{O}$  is similar to the hydrolysis mechanisms for  $\text{BH}_3(\text{OH})^-$  and  $\text{BH}_2(\text{OH})_2^-$ :



The energy barrier along this pathway is 0.59 eV (see the Supporting Information, Figure S21). The computed pathway involves proton shuttling among four  $\text{H}_2\text{O}$  molecules, as can be seen from Figure 12. We note that the mechanism for  $\text{BH}_2(\text{OH})_2^-$  hydrolysis (Figure 8 and the corresponding movie in the Supporting Information) also involves multiple  $\text{H}_2\text{O}$  molecules. After the transition state, the hydride and a proton on a nearby  $\text{H}_2\text{O}$  combine to generate  $\text{H}_2$  and  $\text{OH}^-$ . The  $\text{OH}^-$

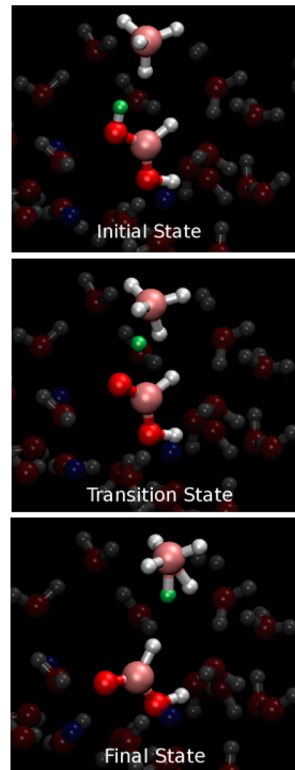


**Figure 11.** Structures of the initial, transition, and final states for reaction between  $\text{BH}(\text{OH})_2$  and  $\text{BH}_4^-$  corresponding to the reaction in eq 13.

in turn receives a proton from  $\text{B}(\text{OH})_3$  to produce  $\text{H}_2\text{O}$  and  $\text{B}(\text{OH})_2\text{O}^-$ . We have not identified a reaction mechanism for hydrated  $\text{BH}(\text{OH})_2$  to produce  $\text{B}(\text{OH})_3 + \text{H}_2$  analogous to eq 11 for hydrated  $\text{BH}_2(\text{OH})$ . Such a mechanism may exist, but given the high barrier for eq 11 and the added steric hindrance of  $\text{BH}(\text{OH})_2$  compared with  $\text{BH}_2(\text{OH})$ , we assume this would be an energetically unfavorable pathway.

The final products will include mixtures of different borates and metaborates, depending on the concentration and pH of the solution. Our calculations show that  $\text{B}(\text{OH})_3$  is metastable in basic solutions and would react with  $\text{OH}^-$  to produce the conjugate base  $\text{B}(\text{OH})_2\text{O}^-$  or the borate anion  $\text{B}(\text{OH})_4^-$  depending on the surrounding solvent structure. We have also shown that  $\text{B}(\text{OH})_2\text{O}^-$  and  $\text{H}_2\text{O}$  can combine to generate  $\text{B}(\text{OH})_4^-$ , which is more energetically favorable than either  $[\text{B}(\text{OH})_2\text{O}^- + \text{H}_2\text{O}]$  or  $[\text{B}(\text{OH})_3 + \text{OH}^-]$ . Our calculations are consistent with the experimental observation that the main product of  $\text{NaBH}_4$  hydrolysis is  $\text{NaB}(\text{OH})_4$ .<sup>37</sup> The bottom of Scheme 1 shows the conversion from  $\text{B}(\text{OH})_3$  to  $\text{B}(\text{OH})_2\text{O}^-$ , and  $\text{B}(\text{OH})_4^-$ .

The energy barrier for reaction (a) (see Scheme 1) is 0.16 eV. The product state is 0.12 eV lower in energy than the reactant state (Figure 13). Thus,  $\text{H}_2\text{O}$  and  $\text{B}(\text{OH})_2\text{O}^-$  formation is thermodynamically favorable and therefore explains why eq 14 is not terminated with  $\text{B}(\text{OH})_3 + \text{OH}^-$ . The energy barrier for reaction (b) is merely 0.1 eV, and the products are 0.73 eV lower in energy than the reactants. Finally, the energy barrier for reaction (c) is 0.37 eV and the product  $\text{B}(\text{OH})_4^-$  is 0.69 eV lower in energy than the reactant  $[\text{B}(\text{OH})_2\text{O}^- + \text{H}_2\text{O}]$ . Movies for these three reactions are given in the Supporting Information.

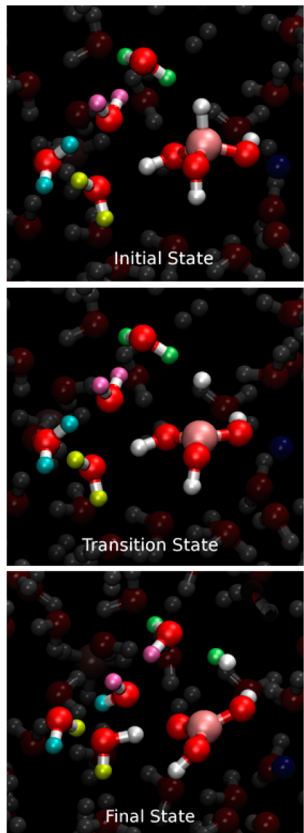


**Figure 12.** Structures of the initial, transition, and final states in hydrolysis of  $\text{BH}(\text{OH})_3^-$  to  $\text{B}(\text{OH})_2\text{O}^-$  (eq 14 and Supporting Information, Figure S21).

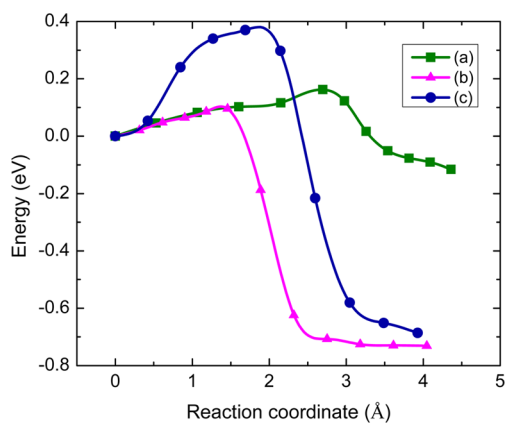


**Figure 13.** Density functional theory CVNEB calculations of the minimum-energy pathways for reactions shown in Scheme 1. (a)  $\text{B}(\text{OH})_3 + \text{OH}^- \rightarrow \text{B}(\text{OH})_2\text{O}^- + \text{H}_2\text{O}$ ; (b)  $\text{B}(\text{OH})_3 + \text{OH}^- \rightarrow \text{B}(\text{OH})_4^-$ ; (c)  $\text{B}(\text{OH})_2\text{O}^- + \text{H}_2\text{O} \rightarrow \text{B}(\text{OH})_4^-$ . Note that the initial states are each set to zero arbitrarily.

## CONCLUSION

We have used a combined approach of high-temperature AIMD and NEB calculations to carry out an unbiased identification of elementary reaction steps for uncatalyzed  $\text{NaBH}_4$  hydrolysis with no *a priori* assumptions about its mechanism. This has enabled us to develop a comprehensive picture of aqueous environment-mediated hydrogen transfers that are relevant for broad classes of proton and/or hydride transfers. Reaction of intermediate hydroxyborates  $\text{BH}_{4-x}(\text{OH})_x^-$  ( $x = 1, 2, 3$ ) and

$\text{H}_2\text{O}$  were identified. The initial step in the hydrolysis proceeds by proton transfer to  $\text{BH}_4^-$  to form  $\text{BH}_5^-$ , which subsequently reacts to form  $\text{BH}_3$  and  $\text{H}_2$ . Importantly, this initial step is fundamentally different from all following steps we have identified in that none of the hydroxyborates form five-coordinate species. Instead, most of the reactions with hydroxyborates involve  $\text{H}_2$  evolving as a result of direct dihydrogen bond formation between the hydroxyborate and water. These reactions also generate transiently stable three-coordinated planar structures having the formula  $\text{BH}_{3-y}(\text{OH})_y$  ( $y = 0, 1, 2$ ).

Most of the reaction pathways we have identified involve extensive proton shuttling along water chains surrounding the hydroxyborate. Our modeling shows these shuttling processes span multiple water molecules extending outside of the first solvation shell. The small size of our simulation cell prevents us from observing longer range proton transport. However, examination of size effects is outside the scope of this work. For reactions that generate a product hydroxyl group, these proton shuttling events act to virtually transport the  $\text{OH}^-$  group away from the other product species so that it forms a hydrogen bond stabilized complex. These reactions involve different numbers of water molecules and should be thought of as representative of the classes of reactions that occur in solution under reaction conditions. Indeed, by noting the characters of the chemical bonds between atom centers involved processes, one can see how these processes would be relatable to diverse areas of chemistry.

The elementary reactions we have identified share a commonality in that they require both protons and hydroxyl ions to proceed to completion. For example, reactions given by eqs 3, 6, 10, and 14 require protons, while reactions given by eqs 5, 9, and 12 require  $\text{OH}^-$  anions. This explains the inhibiting effect of basic solutions.

To the best of our knowledge, this is the most comprehensive computational study to date on elementary mechanisms for the hydrolysis of borohydride. Our unbiased modeling unraveled numerous mechanisms and elucidated which of them were promoted by acids, bases, and which involve 3c-2e moieties analogous to those found in agostic interactions with organometallic catalysts. We note that the absolute barriers reported herein bring some uncertainty arising from the accuracy of DFT, the choice of NEB methodology used, and how comparable calculated barriers at 0 K are to experimental observation (energy differences between barrier heights should be considered to be reasonably accurate though). Moreover, since the actual reaction involves ensembles of pathways that would be accessible at each reaction step due to solvent complexity, one should not place too much emphasis on the actual value of any barriers determined here. We expect these pathways to be similar for hydrolysis of other borohydrides, since the cation was not found to directly participate in any of the reaction mechanisms. Furthermore, we have displayed that using AIMD in tandem with NEB methods can be a powerful approach for modeling complex chemical processes occurring in aqueous phase. Finally, we note that the approach we use to identify complex reaction pathways in condensed phase systems can be used in conjunction with metadynamics to calculate free energies at finite temperatures of each of the reactions. Our approach would provide the insight needed to identify the correct set of collective variables for accurate potential of mean force calculations.

## ■ ASSOCIATED CONTENT

### § Supporting Information

Simulation details, validation of the PW91 functional, comparison of energy pathways computed from CVNEB and G-SSNEB methods, table of reaction barriers and reaction energies from each method, minimum-energy pathway plots, and movies showing the NEB images for many of the reactions. This material is available free of charge via the Internet at <http://pubs.acs.org>.

## ■ AUTHOR INFORMATION

### Notes

The authors declare no competing financial interest.

## ■ ACKNOWLEDGMENTS

The work was funded by the National Science Foundation (Grant No. CBET 0755937) as part of a GOALI project between University of Pittsburgh, University of South Carolina, and Trulite, Inc (El Dorado Hills, CA). We thank K. Grice and M. A. Matthews for many helpful discussions. Computational work was performed at Center for Simulation & Modeling of University of Pittsburgh and Extreme Science and Engineering Discovery Environment (XSEDE) under Project No. TG-DMR110091. J.A.K. graciously acknowledges support from the R. K. Mellon foundation and start up support from the Department of Chemical & Petroleum Engineering at the University of Pittsburgh.

## ■ REFERENCES

- (1) Weinberg, D. R.; Gagliardi, C. J.; Hull, J. F.; Murphy, C. F.; Kent, C. A.; Westlake, B. C.; Paul, A.; Ess, D. H.; McCafferty, D. G.; Meyer, T. J. Proton-Coupled Electron Transfer. *Chem. Rev. (Washington, DC, U.S.)* **2012**, *112*, 4016–4093.
- (2) Costentin, C.; Robert, M.; Savéant, J.-M. Electrochemical and Homogeneous Proton-Coupled Electron Transfers: Concerted Pathways in the One-Electron Oxidation of a Phenol Coupled with an Intramolecular Amine-Driven Proton Transfer. *J. Am. Chem. Soc.* **2006**, *128*, 4552–4553.
- (3) Mayer, J. M. Understanding Hydrogen Atom Transfer: From Bond Strengths to Marcus Theory. *Acc. Chem. Res.* **2010**, *44*, 36–46.
- (4) Hammes-Schiffer, S. Proton-Coupled Electron Transfer: Classification Scheme and Guide to Theoretical Methods. *Energy Environ. Sci.* **2012**, *5*, 7696–7703.
- (5) Hammes-Schiffer, S.; Stuchebrukhov, A. A. Theory of Coupled Electron and Proton Transfer Reactions. *Chem. Rev. (Washington, DC, U.S.)* **2010**, *110*, 6939–6960.
- (6) Zimmerman, P. M.; Zhang, Z.; Musgrave, C. B. Dynamic Mechanisms for Ammonia Borane Thermolysis in Solvent: Deviation from Gas-Phase Minimum-Energy Pathways. *J. Phys. Chem. Lett.* **2011**, *2*, 276–281.
- (7) Comas-Vives, A.; Ujaque, G. Unraveling the Pathway of Gold(I)-Catalyzed Olefin Hydrogenation: An Ionic Mechanism. *J. Am. Chem. Soc.* **2012**, *135*, 1295–1305.
- (8) McSkimming, A.; Colbran, S. B. The Coordination Chemistry of Organo-Hydride Donors: New Prospects for Efficient Multi-Electron Reduction. *Chem. Soc. Rev.* **2013**, *42*, 5439–5488.
- (9) Orimo, S.-i.; Nakamori, Y.; Eliseo, J. R.; Züttel, A.; Jensen, C. M. Complex Hydrides for Hydrogen Storage. *Chem. Rev. (Washington, DC, U.S.)* **2007**, *107*, 4111–4132.
- (10) Sakintuna, B.; Lamari-Darkrim, F.; Hirscher, M. Metal Hydride Materials for Solid Hydrogen Storage: A Review. *Int. J. Hydrogen Energy* **2007**, *32*, 1121–1140.
- (11) Dubois, M. R.; Dubois, D. L. Development of Molecular Electrocatalysts for CO<sub>2</sub> Reduction and H<sub>2</sub> Production/Oxidation. *Acc. Chem. Res.* **2009**, *42*, 1974–1982.
- (12) Bhugun, I.; Lexa, D.; Savéant, J.-M. Homogeneous Catalysis of Electrochemical Hydrogen Evolution by Iron(0) Porphyrins. *J. Am. Chem. Soc.* **1996**, *118*, 3982–3983.
- (13) Wilson, A. D.; Newell, R. H.; McNevin, M. J.; Muckerman, J. T.; Rakowski DuBois, M.; DuBois, D. L. Hydrogen Oxidation and Production Using Nickel-Based Molecular Catalysts with Positioned Proton Relays. *J. Am. Chem. Soc.* **2005**, *128*, 358–366.
- (14) Dempsey, J. L.; Brunschwig, B. S.; Winkler, J. R.; Gray, H. B. Hydrogen Evolution Catalyzed by Cobaloximes. *Acc. Chem. Res.* **2009**, *42*, 1995–2004.
- (15) McEvoy, J. P.; Brudvig, G. W. Structure-Based Mechanism of Photosynthetic Water Oxidation. *Phys. Chem. Chem. Phys.* **2004**, *6*, 4754–4763.
- (16) Dau, H.; Limberg, C.; Reier, T.; Risch, M.; Roggan, S.; Strasser, P. The Mechanism of Water Oxidation: From Electrolysis Via Homogeneous to Biological Catalysis. *ChemCatChem* **2010**, *2*, 724–761.
- (17) Meyer, T. J.; Huynh, M. H. V.; Thorp, H. H. The Possible Role of Proton-Coupled Electron Transfer (Pcet) in Water Oxidation by Photosystem II. *Angew. Chem., Int. Ed.* **2007**, *46*, 5284–5304.
- (18) Rüttinger, W.; Dismukes, G. C. Synthetic Water-Oxidation Catalysts for Artificial Photosynthetic Water Oxidation. *Chem. Rev. (Washington, DC, U.S.)* **1997**, *97*, 1–24.
- (19) Benson, E. E.; Kubiak, C. P.; Sathrum, A. J.; Smieja, J. M. Electrocatalytic and Homogeneous Approaches to Conversion of CO<sub>2</sub> to Liquid Fuels. *Chem. Soc. Rev.* **2009**, *38*, 89–99.
- (20) Morris, A. J.; Meyer, G. J.; Fujita, E. Molecular Approaches to the Photocatalytic Reduction of Carbon Dioxide for Solar Fuels. *Acc. Chem. Res.* **2009**, *42*, 1983–1994.
- (21) Oh, Y.; Hu, X. Organic Molecules as Mediators and Catalysts for Photocatalytic and Electrocatalytic CO<sub>2</sub> Reduction. *Chem. Soc. Rev.* **2013**, *42*, 2253–2261.
- (22) Costentin, C.; Robert, M.; Saveant, J.-M. Catalysis of the Electrochemical Reduction of Carbon Dioxide. *Chem. Soc. Rev.* **2013**, *42*, 2423–2436.
- (23) Appel, A. M.; et al. Frontiers, Opportunities, and Challenges in Biochemical and Chemical Catalysis of CO<sub>2</sub> Fixation. *Chem. Rev. (Washington, DC, U.S.)* **2013**, *113*, 6621–6658.
- (24) D'Ulivo, A. Chemical Vapor Generation by Tetrahydroborate-(III) and Other Borane Complexes in Aqueous Media: A Critical Discussion of Fundamental Processes and Mechanisms Involved in Reagent Decomposition and Hydride Formation. *Spectrochim. Acta, Part B* **2004**, *59*, 793–825.
- (25) Alcantara, A. F. D.; dos Santos Barroso, H.; Pilo-Veloso, D. Reduction of Amides by Boranes. *Quim. Nova* **2002**, *25*, 300–311.
- (26) Cook, M. M.; Halpern, M. E. Use of Phase-Transfer Catalysis in Borohydride Reductions: Review and New Ideas. *Chim. Oggi* **1998**, *16*, 44–48.
- (27) Firouzabadi, H.; Jamalian, A. Reduction of Oxygenated Organosulfur Compounds. *J. Sulfur Chem.* **2008**, *29*, 53–97.
- (28) Gribble, G. W. Sodium Borohydride in Carboxylic Acid Media: A Phenomenal Reduction System. *Chem. Soc. Rev.* **1998**, *27*, 395–404.
- (29) Kas'yan, L. I.; Kas'yan, A. O.; Golodaeva, E. A. Methods and Mechanisms of Epoxy Compounds Reduction. *Russ. J. Org. Chem.* **2008**, *44*, 153–183.
- (30) Kim, J.; Suri, J. T.; Cordes, D. B.; Singaram, B. Asymmetric Reductions Involving Borohydrides: A Practical Asymmetric Reduction of Ketones Mediated by (L)-Tart-NO<sub>2</sub>: A Chiral Lewis Acid. *Org. Process Res. Dev.* **2006**, *10*, 949–958.
- (31) Ma, J.; Choudhury, N. A.; Sahai, Y. A Comprehensive Review of Direct Borohydride Fuel Cells. *Renewable Sustainable Energy Rev.* **2010**, *14*, 183–199.
- (32) Periasamy, M.; Thirumalaikumar, P. Methods of Enhancement of Reactivity and Selectivity of Sodium Borohydride for Applications in Organic Synthesis. *J. Organomet. Chem.* **2000**, *609*, 137–151.
- (33) Purich, D. L. Use of Sodium Borohydride to Detect Acyl-Phosphate Linkages in Enzyme Reactions. In *Enzyme Kinetics and Mechanism, Part F: Detection and Characterization of Enzyme Reaction Intermediates*; Elsevier: Amsterdam, The Netherlands, 2002.354168177

- (34) Santos, D. M. F.; Sequeira, C. A. C. Sodium Borohydride as a Fuel for the Future. *Renewable Sustainable Energy Rev.* **2011**, *15*, 3980–4001.
- (35) Valle-Orta, M.; Diaz, D.; Santiago-Jacinto, P.; Vazquez-Olmos, A.; Reguera, E. Instantaneous Synthesis of Stable Zerovalent Metal Nanoparticles under Standard Reaction Conditions. *J. Phys. Chem. B* **2008**, *112*, 14427–14434.
- (36) Schlesinger, H. I.; Brown, H. C.; Finholt, A. E.; Gilbreath, J. R.; Hoekstra, H. R.; Hyde, E. K. Sodium Borohydride, Its Hydrolysis and Its Use as a Reducing Agent and in the Generation of Hydrogen. *J. Am. Chem. Soc.* **1953**, *75*, 215–219.
- (37) Retnamma, R.; Novais, A. Q.; Rangel, C. M. Kinetics of Hydrolysis of Sodium Borohydride for Hydrogen Production in Fuel Cell Applications: A Review. *Int. J. Hydrogen Energy* **2011**, *36*, 9772–9790.
- (38) Bryant, R. G.; Johnson, M. A.; Rossky, P. J. Water. *Acc. Chem. Res.* **2012**, *45*, 1–2.
- (39) Kaufman, C. M.; Sen, B. Hydrogen Generation by Hydrolysis of Sodium Tetrahydroborate: Effects of Acids and Transition Metals and Their Salts. *J. Chem. Soc., Dalton Trans.* **1985**, 307–313.
- (40) Akdim, O.; Demirci, U. B.; Miele, P. More Reactive Cobalt Chloride in the Hydrolysis of Sodium Borohydride. *Int. J. Hydrogen Energy* **2009**, *34*, 9444–9449.
- (41) Amendola, S. C.; Sharp-Goldman, S. L.; Janjua, M. S.; Spencer, N. C.; Kelly, M. T.; Petillo, P. J.; Binder, M. Safe, Portable, Hydrogen Gas Generator Using Aqueous Borohydride Solution and Ru Catalyst. *Int. J. Hydrogen Energy* **2000**, *25*, 969–975.
- (42) Hung, A. J.; Tsai, S. F.; Hsu, Y. Y.; Ku, J. R.; Chen, Y. H.; Yu, C. C. Kinetics of Sodium Borohydride Hydrolysis Reaction for Hydrogen Generation. *Int. J. Hydrogen Energy* **2008**, *33*, 6205–6215.
- (43) Liu, B. H.; Li, Q. A Highly Active Co-B Catalyst for Hydrogen Generation from Sodium Borohydride Hydrolysis. *Int. J. Hydrogen Energy* **2008**, *33*, 7385–7391.
- (44) Metin, Ö.; Özkar, S. Hydrogen Generation from the Hydrolysis of Sodium Borohydride by Using Water Dispersible, Hydrogenphosphate-Stabilized Nickel(0) Nanoclusters as Catalyst. *Int. J. Hydrogen Energy* **2007**, *32*, 1707–1715.
- (45) Prosini, P. P.; Gislon, P. Water Consumption During Solid State Sodium Borohydride Hydrolysis. *Int. J. Hydrogen Energy* **2010**, *35*, 12234–12238.
- (46) Ding, X. L.; Yuan, X.; Jia, C.; Ma, Z. F. Hydrogen Generation from Catalytic Hydrolysis of Sodium Borohydride Solution Using Cobalt-Copper-Boride (Co-Cu-B) Catalysts. *Int. J. Hydrogen Energy* **2010**, *35*, 11077–11084.
- (47) Demirci, U. B.; Garin, F. Kinetics of Ru-Promoted Sulphated Zirconia Catalysed Hydrogen Generation by Hydrolysis of Sodium Tetrahydroborate. *J. Mol. Catal. A: Chem.* **2008**, *279*, 57–62.
- (48) Li, F.; Li, Q.; Kim, H. CoB/Open-Cnts Catalysts for Hydrogen Generation from Alkaline NaBH<sub>4</sub> Solution. *Chem. Eng. J.* **2012**, *210*, 316–324.
- (49) Liang, Y.; Wang, P.; Dai, H. B. Hydrogen Bubbles Dynamic Template Preparation of a Porous Fe-Co-B/Ni Foam Catalyst for Hydrogen Generation from Hydrolysis of Alkaline Sodium Borohydride Solution. *J. Alloys Compd.* **2010**, *491*, 359–365.
- (50) Oh, T. H.; Kwon, S. Effect of Manufacturing Conditions on Properties of Electroless Deposited Co-P/Ni Foam Catalyst for Hydrolysis of Sodium Borohydride Solution. *Int. J. Hydrogen Energy* **2012**, *37*, 15925–15937.
- (51) Peng, S. G.; Liu, C. Y.; Liu, X. F.; Zhang, J.; Zhang, Y. Q. Water Dispersible Ru (0) Nanorods: A Highly Efficient Heterogeneous Catalyst for the Hydrogen Generation from Sodium Borohydride Solutions. *Integr. Ferroelectr.* **2012**, *135*, 47–54.
- (52) Aiello, R.; Sharp, J. H.; Matthews, M. A. Production of Hydrogen from Chemical Hydrides Via Hydrolysis with Steam. *Int. J. Hydrogen Energy* **1999**, *24*, 1123–1130.
- (53) Marrero-Alfonso, E. Y.; Gray, J. R.; Davis, T. A.; Matthews, M. A. Hydrolysis of Sodium Borohydride with Steam. *Int. J. Hydrogen Energy* **2007**, *32*, 4717–4722.
- (54) Marrero-Alfonso, E. Y.; Gray, J. R.; Davis, T. A.; Matthews, M. A. Minimizing Water Utilization in Hydrolysis of Sodium Borohydride: The Role of Sodium Metaborate Hydrates. *Int. J. Hydrogen Energy* **2007**, *32*, 4723–4730.
- (55) Andrieux, J.; Demirci, U. B.; Hannauer, J.; Gervais, C.; Goutaudier, C.; Miele, P. Spontaneous Hydrolysis of Sodium Borohydride in Harsh Conditions. *Int. J. Hydrogen Energy* **2011**, *36*, 224–233.
- (56) Kilpatrick, M.; McKinney, C. D. Kinetics of the Reaction of Lithium Borohydride in Aqueous Acid Solution. *J. Am. Chem. Soc.* **1950**, *72*, 5474–5476.
- (57) Mikheeva, V. I.; Surs, V. Y. O Khimicheskoi Prirode Gipoborata Kaliya. *Dokl. Akad. Nauk SSSR* **1953**, *93*, 67–69.
- (58) Mikheeva, V. I.; Surs, V. Y. O Reaktsii Borida Magniya S Vodoi. *Dokl. Akad. Nauk SSSR* **1953**, *91*, 1133–1135.
- (59) Pecsok, R. L. Polarographic Studies on the Oxidation and Hydrolysis of Sodium Borohydride. *J. Am. Chem. Soc.* **1953**, *75*, 2862–2864.
- (60) Castellan, G. W. Symmetry and Stability in Diborane and in Borine. *J. Chem. Phys.* **1954**, *22*, 536–538.
- (61) Mikheeva, V. I.; Fedneva, E. M. O Gidrolize Borogidrida Litiya. *Dokl. Akad. Nauk SSSR* **1955**, *101*, 99–101.
- (62) Brown, J.; Svensson, M. Additions and Corrections: The Stability of Potassium Borohydride in Alkaline Solutions. *J. Am. Chem. Soc.* **1957**, *79*, 6581–6581.
- (63) Brown, J. B.; Svensson, M. The Stability of Potassium Borohydride in Alkaline Solutions. *J. Am. Chem. Soc.* **1957**, *79*, 4241–4242.
- (64) Freund, T. Kinetics of the Reduction of Inorganic Ions by Borohydride. I. Ferricyanide. *J. Inorg. Nucl. Chem.* **1959**, *9*, 246–251.
- (65) Goubeau, J.; Kalfass, H. Die Reaktion Natriumborhydrid Und Wasser. *Z. Anorg. Allg. Chem.* **1959**, *299*, 160–169.
- (66) Davis, R. E.; Kirby, C. L.; Swain, C. G. An Inverse Hydrogen Isotope Effect in the Hydrolysis of Sodium Borohydride. *J. Am. Chem. Soc.* **1960**, *82*, 5950–5951.
- (67) Davis, R. E.; Swain, C. G. General Acid Catalysis of the Hydrolysis of Sodium Borohydride. *J. Am. Chem. Soc.* **1960**, *82*, 5949–5950.
- (68) Mochalov, K. N.; Gil'manshin, G. G. Polarographic Behaviour of Sodium, Potassium and Lithium Boronhydrides. *Dokl. Akad. Nauk SSSR* **1960**, *132*, 134–137.
- (69) Stockmayer, W. H.; Miller, R. R.; Zeto, R. J. Kinetics of Borohydride Hydrolysis. *J. Phys. Chem.* **1961**, *65*, 1076–1077.
- (70) Davis, R. E.; Bromels, E.; Kirby, C. L. Boron Hydrides. III. Hydrolysis of Sodium Borohydride in Aqueous Solution. *J. Am. Chem. Soc.* **1962**, *84*, 885–892.
- (71) Mesmer, R. E.; Jolly, W. L. Hydrolysis of Aqueous Hydroborate. *Inorg. Chem.* **1962**, *1*, 608–612.
- (72) Gardiner, J. A.; Collat, J. W. The Hydrolysis of Sodium Tetrahydroborate. Identification of an Intermediate. *J. Am. Chem. Soc.* **1964**, *86*, 3165–3166.
- (73) Gardiner, J. A.; Collat, J. W. Kinetics of the Stepwise Hydrolysis of Tetrahydroborate Ion. *J. Am. Chem. Soc.* **1965**, *87*, 1692–1700.
- (74) Gardiner, J. A.; Collat, J. W. Polarography of the Tetrahydroborate Ion. The Effect of Hydrolysis on the System. *Inorg. Chem.* **1965**, *4*, 1208–1212.
- (75) Mochalov, K. N.; Khain, V. S.; Gil'manshin, G. G. A Generalized Scheme for Hydrolysis of Borohydride Ion and Diborane. *Dokl. Akad. Nauk SSSR* **1965**, *162*, 402–406.
- (76) Mochalov, K. N.; Khain, V. S.; Gil'manshin, G. G. Kinetic Studies on Intermediate Steps of BH<sub>4</sub><sup>-</sup> Hydrolysis. *Kinet. Katal.* **1965**, *6*, 541–544.
- (77) Kreevoy, M. M.; Hutchins, J. E. H<sub>2</sub>BH<sub>3</sub> as an Intermediate in Tetrahydridoborate Hydrolysis. *J. Am. Chem. Soc.* **1972**, *94*, 6371–6376.
- (78) Wang, F. T.; Jolly, W. L. A Kinetic Study of the Intermediates in the Hydrolysis of the Hydroborate Ion. *Inorg. Chem.* **1972**, *11*, 1933–1941.

- (79) Zhang, Q.; Mohring, R. M. Reaction Chemistry between Aqueous Sulfuric Acid and Solid Sodium Borohydride. *Ind. Eng. Chem. Res.* **2009**, *48*, 1603–1607.
- (80) Akdim, O.; Demirci, U. B.; Miele, P. Acetic Acid, a Relatively Green Single-Use Catalyst for Hydrogen Generation from Sodium Borohydride. *Int. J. Hydrogen Energy* **2009**, *34*, 7231–7238.
- (81) Murugesan, S.; Subramanian, V. Effects of Acid Accelerators on Hydrogen Generation from Solid Sodium Borohydride Using Small Scale Devices. *J. Power Sources* **2009**, *187*, 216–223.
- (82) Minkina, V. G.; Shabunya, S. I.; Kalinin, V. I.; Martynenko, V. V. Stability of Aqueous-Alkaline Sodium Borohydride Formulations. *Russ. J. Appl. Chem.* **2008**, *81*, 380–385.
- (83) Minkina, V. G.; Shabunya, S. I.; Kalinin, V. I.; Martynenko, V. V.; Smirnova, A. L. Long-Term Stability of Sodium Borohydrides for Hydrogen Generation. *Int. J. Hydrogen Energy* **2008**, *33*, 5629–5635.
- (84) Moon, G. Y.; Lee, S. S.; Lee, K. Y.; Kim, S. H.; Song, K. H. Behavior of Hydrogen Evolution of Aqueous Sodium Borohydride Solutions. *J. Ind. Eng. Chem.* **2008**, *14*, 94–99.
- (85) Urgnani, J.; Torres, F. J.; Palumbo, M.; Baricco, M. Hydrogen Release from Solid State NaBH<sub>4</sub>. *Int. J. Hydrogen Energy* **2008**, *33*, 3111–3115.
- (86) Hohenberg, P.; Kohn, W. Inhomogeneous Electron Gas. *Phys. Rev.* **1964**, *136*, B864–B871.
- (87) Kohn, W.; Sham, L. J. Self-Consistent Equations Including Exchange and Correlation Effects. *Phys. Rev.* **1965**, *140*, A1133–A1138.
- (88) Kresse, G.; Furthmüller, J. Efficiency of Ab-Initio Total Energy Calculations for Metals and Semiconductors Using a Plane-Wave Basis Set. *Comput. Mater. Sci.* **1996**, *6*, 15–50.
- (89) Kresse, G.; Furthmüller, J. Efficient Iterative Schemes for Ab Initio Total-Energy Calculations Using a Plane-Wave Basis Set. *Phys. Rev. B* **1996**, *54*, 11169–11186.
- (90) Kresse, G.; Hafner, J. Ab Initio Molecular Dynamics for Liquid Metals. *Phys. Rev. B* **1993**, *47*, 558–561.
- (91) Kresse, G.; Hafner, J. Ab Initio Molecular-Dynamics Simulation of the Liquid-Metalamorphous-Semiconductor Transition in Germanium. *Phys. Rev. B* **1994**, *49*, 14251–14269.
- (92) Perdew, J. P.; Chevary, J. A.; Vosko, S. H.; Jackson, K. A.; Pederson, M. R.; Singh, D. J.; Fiolhais, C. Atoms, Molecules, Solids, and Surfaces: Applications of the Generalized Gradient Approximation for Exchange and Correlation. *Phys. Rev. B* **1992**, *46*, 6671–6687.
- (93) Perdew, J. P.; Chevary, J. A.; Vosko, S. H.; Jackson, K. A.; Pederson, M. R.; Singh, D. J.; Fiolhais, C. Erratum: Atoms, Molecules, Solids, and Surfaces: Applications of the Generalized Gradient Approximation for Exchange and Correlation. *Phys. Rev. B* **1993**, *48*, 4978.
- (94) Blöchl, P. E. Projector Augmented-Wave Method. *Phys. Rev. B* **1994**, *50*, 17953–17979.
- (95) Kresse, G.; Joubert, D. From Ultrasoft Pseudopotentials to the Projector Augmented-Wave Method. *Phys. Rev. B* **1999**, *59*, 1758–1775.
- (96) Cohen, A. J.; Mori-Sánchez, P.; Yang, W. Insights into Current Limitations of Density Functional Theory. *Science* **2008**, *321*, 792–794.
- (97) VandeVondele, J.; Mohamed, F.; Krack, M.; Hutter, J.; Sprik, M.; Parrinello, M. The Influence of Temperature and Density Functional Models in Ab Initio Molecular Dynamics Simulation of Liquid Water. *J. Chem. Phys.* **2005**, *122*, 014515.
- (98) Laasonen, K.; Sprik, M.; Parrinello, M.; Car, R. “Ab initio” Liquid Water. *J. Chem. Phys.* **1993**, *99*, 9080–9089.
- (99) Schwegler, E.; Grossman, J. C.; Gygi, F.; Galli, G. Towards an Assessment of the Accuracy of Density Functional Theory for First Principles Simulations of Water. II. *J. Chem. Phys.* **2004**, *121*, 5400–5409.
- (100) Sprik, M.; Hutter, J.; Parrinello, M. Ab initio Molecular Dynamics Simulation of Liquid Water: Comparison of Three Gradient-Corrected Density Functionals. *J. Chem. Phys.* **1996**, *105*, 1142–1152.
- (101) Vassilev, P.; Hartnig, C.; Koper, M. T. M.; Frechard, F.; Van Santen, R. A. Ab Initio Molecular Dynamics Simulation of Liquid Water and Water-Vapor Interface. *J. Chem. Phys.* **2001**, *115*, 9815–9820.
- (102) Leung, K.; Rempe, S. B. Ab Initio Molecular Dynamics Study of Formate Ion Hydration. *J. Am. Chem. Soc.* **2004**, *126*, 344–351.
- (103) Knizia, G.; Adler, T. B.; Werner, H.-J. Simplified CCSD(T)-F12 Methods: Theory and Benchmarks. *J. Chem. Phys.* **2009**, *130*, 054104.
- (104) Cárdenas, R.; Lagúnez-Otero, J.; Flores-Rivero, A. Ab Initio Study of the Reaction Mechanism of Water Dissociation into the Ionic Species OH<sup>−</sup> and H<sub>3</sub>O<sup>+</sup>. *Int. J. Quantum Chem.* **1998**, *68*, 253–259.
- (105) Keith, J. A.; Carter, E. A. Electrochemical Reactivities of Pyridinium in Solution: Consequences for CO<sub>2</sub> Reduction Mechanisms. *Chem. Sci.* **2013**, *4*, 1490–1496.
- (106) Tomasi, J.; Persico, M. Molecular Interactions in Solution: An Overview of Methods Based on Continuous Distributions of the Solvent. *Chem. Rev. (Washington, DC, U.S.)* **1994**, *94*, 2027–2094.
- (107) Tomasi, J.; Mennucci, B.; Cammi, R. Quantum Mechanical Continuum Solvation Models. *Chem. Rev. (Washington, DC, U.S.)* **2005**, *105*, 2999–3094.
- (108) Cramer, C. J.; Truhlar, D. G. Implicit Solvation Models: Equilibria, Structure, Spectra, and Dynamics. *Chem. Rev. (Washington, DC, U.S.)* **1999**, *99*, 2161–2200.
- (109) Pliego, J. R.; Riveros, J. M. The Cluster–Continuum Model for the Calculation of the Solvation Free Energy of Ionic Species. *J. Phys. Chem. A* **2001**, *105*, 7241–7247.
- (110) Martin, R. L.; Hay, P. J.; Pratt, L. R. Hydrolysis of Ferric Ion in Water and Conformational Equilibrium. *J. Phys. Chem. A* **1998**, *102*, 3565–3573.
- (111) Bryantsev, V. S.; Diallo, M. S.; Goddard, W. A., III Calculation of Solvation Free Energies of Charged Solutes Using Mixed Cluster/Continuum Models. *J. Phys. Chem. B* **2008**, *112*, 9709–9719.
- (112) Lim, C.-H.; Holder, A. M.; Musgrave, C. B. Mechanism of Homogeneous Reduction of CO<sub>2</sub> by Pyridine: Proton Relay in Aqueous Solvent and Aromatic Stabilization. *J. Am. Chem. Soc.* **2012**, *135*, 142–154.
- (113) Siegbahn, P. E. M. Two, Three, and Four Water Chain Models for the Nucleophilic Addition Step in the Wacker Process. *J. Phys. Chem.* **1996**, *100*, 14672–14680.
- (114) Mattioli, G.; Giannozzi, P.; Amore Bonapasta, A.; Guidoni, L. Reaction Pathways for Oxygen Evolution Promoted by Cobalt Catalyst. *J. Am. Chem. Soc.* **2013**, *135*, 15353–15363.
- (115) Laio, A.; Parrinello, M. Escaping Free-Energy Minima. *Proc. Natl. Acad. Sci. U.S.A.* **2002**, *99*, 12562–12566.
- (116) Leung, K.; Nielsen, I. M. B.; Sai, N.; Medforth, C.; Shelnutt, J. A. Cobalt–Porphyrin Catalyzed Electrochemical Reduction of Carbon Dioxide in Water. 2. Mechanism from First Principles. *J. Phys. Chem. A* **2010**, *114*, 10174–10184.
- (117) Vallés-Pardo, J. L.; Guijt, M. C.; Iannuzzi, M.; Joya, K. S.; de Groot, H. J. M.; Buda, F. Ab Initio Molecular Dynamics Study of Water Oxidation Reaction Pathways in Mono-Ru Catalysts. *Chem-PhysChem* **2012**, *13*, 140–146.
- (118) Vartak, S.; Roudgar, A.; Golovnev, A.; Eikerling, M. Collective Proton Dynamics at Highly Charged Interfaces Studied by Ab Initio Metadynamics. *J. Phys. Chem. B* **2012**, *117*, 583–588.
- (119) Nair, N. N.; Schreiner, E.; Marx, D. Glycine at the Pyrite–Water Interface: The Role of Surface Defects. *J. Am. Chem. Soc.* **2006**, *128*, 13815–13826.
- (120) Comas-Vives, A.; Stirling, A.; Lledós, A.; Ujaque, G. The Wacker Process: Inner- or Outer-Sphere Nucleophilic Addition? New Insights from Ab Initio Molecular Dynamics. *Chem.—Eur. J.* **2010**, *16*, 8738–8747.
- (121) Sheppard, D.; Xiao, P. H.; Chemelewski, W.; Johnson, D. D.; Henkelman, G. A Generalized Solid-State Nudged Elastic Band Method. *J. Chem. Phys.* **2012**, *136*, 074103.
- (122) Henkelman, G.; Uberuaga, B. P.; Jonsson, H. A Climbing Image Nudged Elastic Band Method for Finding Saddle Points and Minimum Energy Paths. *J. Chem. Phys.* **2000**, *113*, 9901–9904.

- (123) Sheppard, D.; Terrell, R.; Henkelman, G. Optimization Methods for Finding Minimum Energy Paths. *J. Chem. Phys.* **2008**, *128*, 134106.
- (124) Jónsson, H.; Mills, G.; Jacobsen, K. W. *Classical and Quantum Dynamics in Condensed Phase Simulations*; World Scientific: Singapore, 1998; pp 385–404.
- (125) Reed, C. A. Myths About the Proton. The Nature of  $\text{H}^+$  in Condensed Media. *Acc. Chem. Res.* **2013**, *46*, 2567–2575.
- (126) Zhang, J.; Fisher, T. S.; Gore, J. P.; Hazra, D.; Ramachandran, P. V. Heat of Reaction Measurements of Sodium Borohydride Alcoholysis and Hydrolysis. *Int. J. Hydrogen Energy* **2006**, *31*, 2292–2298.
- (127) Damjanović, L.; Bennici, S.; Auroux, A. A Direct Measurement of the Heat Evolved During the Sodium and Potassium Borohydride Catalytic Hydrolysis. *J. Power Sources* **2010**, *195*, 3284–3292.
- (128) Pepperberg, I. M.; Halgren, T. A.; Lipscomb, W. N. A Molecular Orbital Study of the Role of  $\text{BH}_5^-$  in the Hydrolysis of  $\text{BH}_4^-$ . *J. Am. Chem. Soc.* **1976**, *98*, 3442–3451.
- (129) Willem, R. Possible Mechanisms of the Reaction between Tetrahydroborate and Hydrogen Ions: A Permutational Analysis. *J. Chem. Soc., Dalton Trans.* **1979**, 33–40.
- (130) Tuckerman, M. E.; Marx, D.; Parrinello, M. The Nature and Transport Mechanism of Hydrated Hydroxide Ions in Aqueous Solution. *Nature* **2002**, *417*, 925–929.
- (131) Tuckerman, M.; Laasonen, K.; Sprik, M.; Parrinello, M. Ab Initio Molecular Dynamics Simulation of the Solvation and Transport of Hydronium and Hydroxyl Ions in Water. *J. Chem. Phys.* **1995**, *103*, 150–161.
- (132) Hoheisel, C.; Kutzelnigg, W. Ab Initio Calculation Including Electron Correlation of the Structure and Binding Energy of  $\text{BH}_5^-$  and  $\text{B}_2\text{H}_7^-$ . *J. Am. Chem. Soc.* **1975**, *97*, 6970–6975.
- (133) Stanton, J. F.; Lipscomb, W. N.; Bartlett, R. J. A Theoretical Investigation of the Structure and Properties of  $\text{BH}_5^-$ . *J. Am. Chem. Soc.* **1989**, *111*, 5173–5180.
- (134) Shabunya, S. I.; Nesteruk, A. A. Hydrolysis of Aqueous-Alkaline Solutions of Sodium Borohydride. Asymptotics of Low Concentrations of the Alkali. *J. Eng. Phys. Thermophys.* **2012**, *85*, 73–78.
- (135) Agmon, N. The Grotthuss Mechanism. *Chem. Phys. Lett.* **1995**, *244*, 456–462.
- (136) Garrett, B. C.; et al. Role of Water in Electron-Initiated Processes and Radical Chemistry: Issues and Scientific Advances. *Chem. Rev. (Washington, DC, U.S.)* **2005**, *105*, 355–389.
- (137) Burns, W. G.; Moore, P. B. Water Radiolysis and Its Effect Upon in Reactor Zircaloy Corrosion. *Radiat. Eff.* **1976**, *30*, 233–242.
- (138) Chatterjee, A.; Magee, J. L.; Dey, S. K. The Role of Homogeneous Reactions in the Radiolysis of Water. *Radiat. Res.* **1983**, *96*, 1–19.
- (139) Bakker, H. J.; Nienhuys, H. K. Delocalization of Protons in Liquid Water. *Science* **2002**, *297*, 587–590.
- (140) Di Pietro, E.; Cardini, G.; Schettino, V. Ab Initio Molecular Dynamics Study of the Hydrolysis Reaction of Diborane. *Phys. Chem. Chem. Phys.* **2007**, *9*, 3857–3863.
- (141) Carter, E. A.; Ciccotti, G.; Hynes, J. T.; Kapral, R. Constrained Reaction Coordinate Dynamics for the Simulation of Rare Events. *Chem. Phys. Lett.* **1989**, *156*, 472–477.
- (142) Mones, L.; Csányi, G. Topologically Invariant Reaction Coordinates for Simulating Multistate Chemical Reactions. *J. Phys. Chem. B* **2012**, *116*, 14876–14885.